Chronological and Archaeometric Evaluation of Bricks from Archaeological Sites of Upper Assam, Northeast India: Estimation of the Firing Temperature and Civilization History

Raktim Ranjan Saikia , Chaitra Dhar Taye , Nurul Amin , Sorat Konwar , Laura Panzeri * , Anna Galli

Posted Date: 14 June 2024

doi: 10.20944/preprints202406.0997.v1

Keywords: Firing Temperature; XRD-FTIR; SEM-EDS; Archaeometry; Ancient Bricks; TL/OSL dating

 doi:10.20944/preprints202406.0997.v1

Article

Chronological and Archaeometric Evaluation of Bricks from Archaeological Sites of Upper Assam, Northeast India: Estimation of the Firing Temperature and Civilization History

Raktim Ranjan Saikia [1], Chaitra Dhar Taye [1], Nurul Amin [1], Sorat Konwar [1], Laura Panzeri [2] and Anna Galli [2]

[1] Department of Geology, Jagannath Barooah College, Jorhat, 785001, India
[2] Dipartimento di Scienza dei Materiali, Università degli Studi di Milano-Bicocca, Via R. Cozzi 55, 20125 Milano (Italy)
* Correspondence: laura.panzeri@unimib.it

Abstract: This study aims to uncover the chronology and production technologies of ancient bricks unearthed from various locations in Upper Assam, Northeast India. To achieve this goal, complementary spectroscopic techniques such as Fourier Transform Infrared (FTIR), X-ray Diffraction (XRD), Scanning Electron Microscope (SEM) coupled with Energy Dispersive Spectrometer (EDS), as well as Thermoluminescence (TL) and Optically Stimulated Luminescence (OSL/IRSL) dating have been applied. FTIR and XRD analyses revealed the presence of quartz, feldspar (microcline, orthoclase, albite), kaolinite, chlorite, cerussite, palygorskite, magnetite, hematite, and organic carbon. The mineralogical composition indicates two distinct groups with firing temperatures below 650°C and above ~800°C. These two groups could be the first indication of the presence of two civilizations or at least two different production technologies, involving different firing temperatures and kiln atmospheric conditions. Further, the SEM-EDS study suggests that both calcareous and non-calcareous clays were used in brick making, which have low and high refractory properties, respectively. The internal morphology of the samples shows the existence of micropores and microfractures, indicating the influence of higher temperature firing. Absolute dating techniques associate the two brick groups with different age ranges: a firing temperature above ~800°C indicates a superior technology corresponding to a production period between the 7th and 10th centuries CE. In contrast, a temperature below 650°C indicates a technologically less advanced group of people, with the age group dated between the 11th and 14th centuries CE.

Keywords: firing temperature; XRD-FTIR; SEM-EDS; archaeometry; ancient bricks; TL/OSL dating

1. Introduction

The history of human civilization is inherently connected to the utilisation of bricks as a basic building material. Since the third century BCE, there have been numerous structures that use fired or burned bricks (Weaver, 1997). The chronicles of ancient civilizations give evidence to the enduring legacy of brick creation, and several studies infer that the qualities and durability of bricks are closely related to the quality of raw materials, manufacturing techniques such as firing temperature and many other factors (Fernandes et al., 2010; Johari et al., 2010; Mostaghelchi et al., 2013; Rasmussen et al., 2012). Firing temperature is recognized an important factor in brick production because burning triggers significant changes in mineralogy, texture, and physical properties, by impacting the porosity and pore dispersion of bricks (Job Ajala et al., 2016, 2017; Karaman et al., 2006; Velraj et al., 2009).

When clays are fired to make pottery, new minerals called firing minerals are formed. These products are primarily determined by the composition of the clays, the additives used to make pottery, the atmospheric conditions, and the duration of firing during pottery making. Gehlenite and

 doi:10.20944/preprints202406.0997.v1

diopside are high-temperature firing minerals. Gehlenite is formed at 800-850°C from illite and calcite decomposition products (Maritan et al., 2006) and calcite decomposition begins at 650°C and ends at 850°C, giving rise to new high-temperature calco-silicates and aluminum-calcium silicates such as pyroxene group members (diopside) and plagioclase feldspars (anorthite) (İssi et al., 2011; Papachristodoulou et al., 2006). The reaction between quartz and lime at 920 or 1000°C, depending on the quartz content, produced wollastonite. Wollastonite was discovered to replace gehlenite in the gehlenite bearing system at temperatures above 830°C (Böhme et al., 2019). Multidimensional approaches like X-ray powder Diffraction (XRD), Fourier Transform Infrared Spectroscopy (FTIR), Differential Thermal Analysis (DTA) and Scanning Electron Microscopy (SEM) have been demonstrated to be very effective in understanding the firing temperature (Ghale et al., 2019; Keller & Pickett, 1949; Legodi & De Waal, 2007; Mendelovici, 1997; Rasmussen et al., 2012; Rutherford et al., 2012; Velraj et al., 2014). Moreover, the Thermoluminescence (TL) and Optically Stimulated Luminescence (OSL) dating techniques are essential for establishing the time elapsed since the last high-temperature event, which usually coincides with the bricks' firing in a kiln (Aitken, 1985, 1998). The TL and OSL exploit the accumulation of charge carriers in mineral defects, providing a timeline for brick usage and reuse (Galli et al., 2006, 2020).

In India, most investigations have focussed on the ancient architectures of southern part of the country, utilizing similar methodologies to understand the effects of firing temperature and the physic-mechanical properties of ancient bricks (Dhanapandian et al., 2010; Govindasamy et al., 2019a; Kiruba & Ganesan, 2015; Raja Annamalai et al., 2014; V. Ramasamy et al., 2009; Ravisankar et al., 2013, 2014; Velraj et al., 2010, 2014). However, only one notable study analyzed the bricks of the Kamakhya Temple using XRD and FTIR techniques, revealing variations in firing temperatures (above and below 500°C) (Sheikh and Barua, 2013). Except for this, no archaeometry and dating of ancient artefacts from the region has been carried out so far. Hence, the present study aims to fill this gap by focusing on different archaeological sites of Upper Assam, to estimate technological parameters of bricks production such as raw materials used in manufacturing and the firing temperature using FTIR, XRD, and SEM-EDX techniques. Additionally, TL, OSL and IRSL) dating methods will be employed to determine the chronology and historical context of the Dihing Valley and nearby areas of Upper Assam. In this way it is possible to establish whether different brick production technologies exist and, thanks to the determination of an absolute chronology, determine the technological progress that has occurred in the bricks production.

1.1. Study Area

In recent years few important archaeological structures framed with bricks were noticed in four archaeological sites of Upper Assam. (Figure-1). The locations and details of the archaeological sites are described below.

Preprints.org (www.preprints.org) | NOT PEER-REVIEWED | Posted: 14 June 2024 doi:10.20944/preprints202406.0997.v1

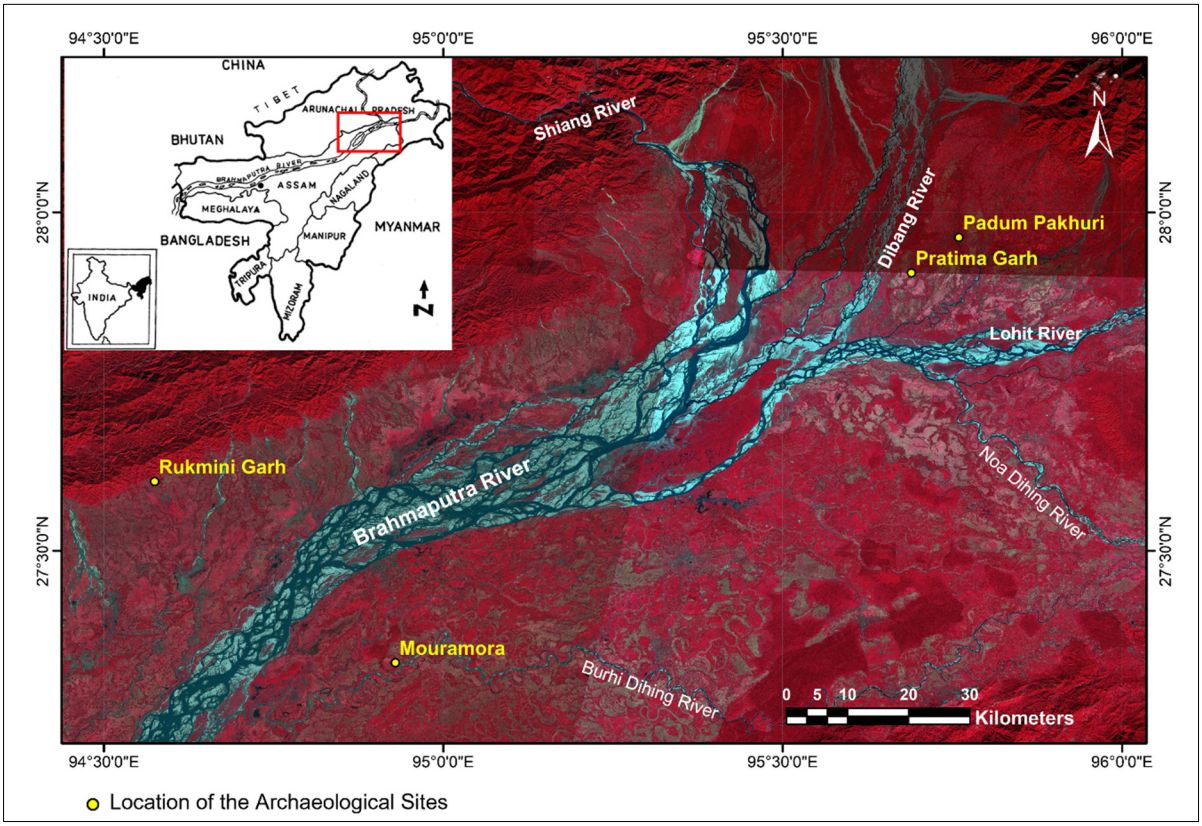

Figure 1. Location map of the study area indicating archaeological sites.

1.1.1. Mouramora Archaeological Spot

Mouramora is situated on the bank of a palaeo-channel of the River Dihing of Dibrugarh District of Assam, India having latitude 27°20'7.051″ and longitude 94°55'45.512″. It was excavated by the Archaeological Survey of Assam in the year 2017. The unearthed structure looks like a plinth of an old temple, may be constructed on the bank of old River Dihing, now found as palaeo-channel of it (Figure-2a). The structure is built with a various shaped and sized bricks with sharp and curve edges (Figure-2b). The bricks have different size that range from 30 cm × 21 cm to about 15 cm × 15 cm with a thickness of about 5 cm. The morphology of the structure and its structural arrangement indicates that it was prepared by a well-organized group of people. A total of three samples of different shape and size have been collected from the site for this work.

 doi:10.20944/preprints202406.0997.v1

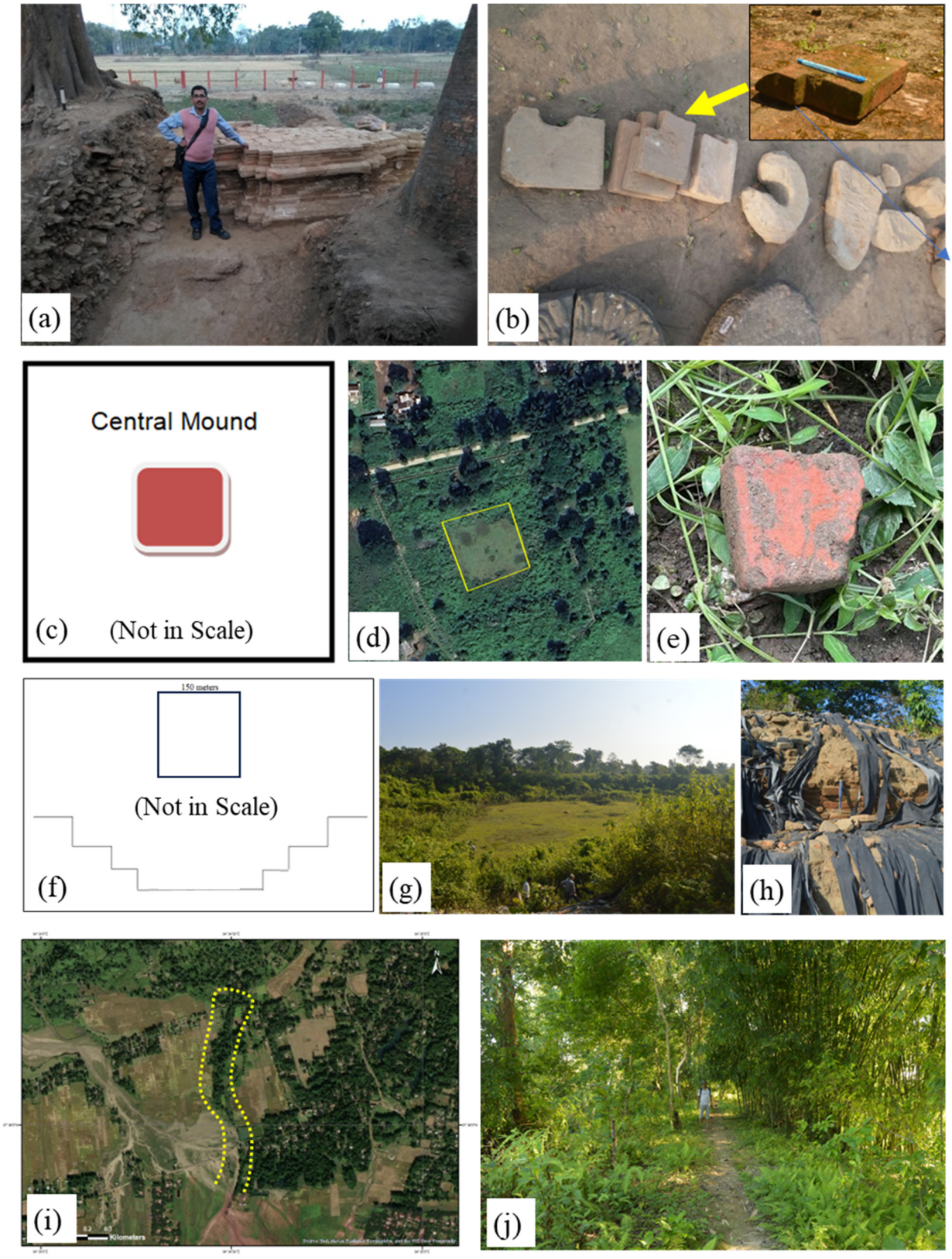

Figure 2. Representative field photograph of four archaeological site, (a) Plinth like old temple structure of Mouramora; (b) Flat and varied shaped bricks used to make plinth like structure of Mouramora; (c) Sketch of the sample point of central mould structure of ancient Pratima Garh; (d) Satellite image representing remnants of central mould structure of ancient Pratima Garh; (e) Close up view of collected samples of Pratima Garh; (f) Top view sketch and cross sectional profile of the ancient tank of Padum Pukhuri; (g) Field photographs showing vegetation-covered Padum Pukhuri

 doi:10.20944/preprints202406.0997.v1

and (h) Intake bricks on the bank of Padum Pukhuri; (i) Satellite image representing remnants of long defensive embankment of Rukmini Garh; and (j) Field photographs of poorly preserved ancient embankment of Rukmini Garh with sample photographs (inset). .

1.1.2. Pratima Garh Archaeological Spot

Pratima Garh is a square shaped defensive barricade located in the Sadiya of Tinsukia district of Assam, India having a latitude 27°54'41.400″ and longitude 95°41'25.500″ The length of one side of the barricade is measured almost 300 meters. There is an almost 4.5-meter-high central mound structure (Figure-2c). Although the site is yet not excavated, one brick sample from this central mound was collected for the present study (Figure-2d and 2e).

1.1.3. Padum Pukhuri Archaeological Spot

The studied location is situated in the Sadiya near the Assam-Arunachal state boarder, India having a latitude 27°57'48.110″ and longitude 95°45'40.000″. It is an ancient tank with bank, fortified with bricks. It is a square shaped dry tank structure. The freshly measured depth of the tank is 3 meters and length of its one side is 150 meters (Figure-2f). Systematic excavation of this pond is not yet started. The brick sample has been collected from the bank of the tank for the present study (Figure-2g and 2h).

1.1.4. Rukmini Garh Archaeological Spot

Rukmini Garh is positioned in the Dhemaji district of Assam, India having a latitude 27°36'11.933″ and longitude 94°34'28.817″. It is a 550-meter (as preserve today) long defensive embankment started from foot hills of Eastern Himalayan (Arunachal-Himalaya) region, and is aligning along North-South direction (Figure-2i). It is assumed that it was originally much longer in length. But due to the seasonal flood by Jokai River (neighbouring river), only 550-meter-long area is remained in poor condition. The construction pattern of the structure is uncommon. At first a core brick wall was constructed and the wall was covered with a thick cover of soil. The core brick wall and the soil cover together made a strong defensive embankment. Samples from the core of the embankment have been collected for the study (Figure-2j). This place is not excavated yet.

2. Materials and Methods

To achieve the goal of the present study six brick samples have been collected from the specified archaeological sites of Upper Assam (three from Mouramora, one each from Pratima Garh, Rukmini Garh and Padum Pukhuri). The collected samples are studied systematically using the following procedures.

2.1. Colour of the Brick's Identification

The colour of the brick has been identified using the Munsell colour chart, 1994 revised edition. All the samples from the Mouramora site, called Mouramora 1, 2, and 3, show a light red colour (7/6, HUE 2.5 YR). Other samples, such as Padum Pukhuri, Rukmini Garh, and Pratima Garh, display light red (6/6, HUE 10R), reddish yellow (6/6, HUE 5 YR), and weak red (5/4, HUE 10R) colours, respectively (Figure-3).

 doi:10.20944/preprints202406.0997.v1

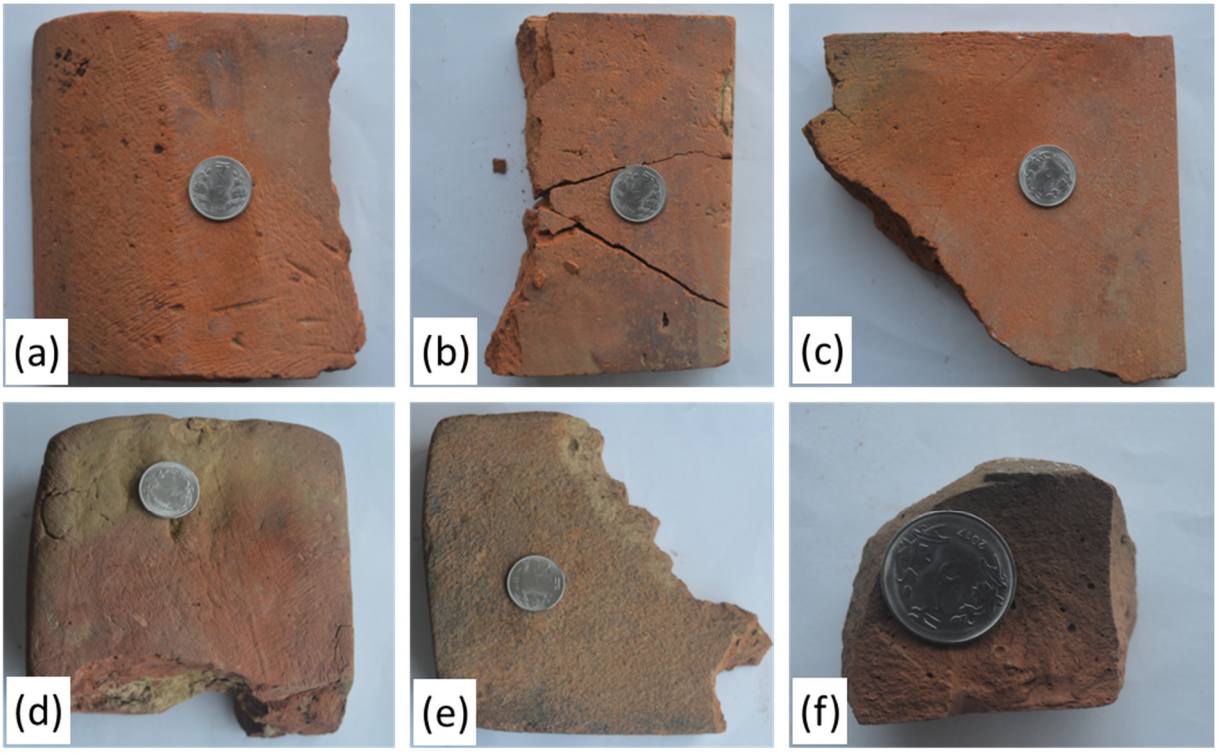

Figure 3. Photograph representing colour of the bricks of four archaeological site: (a-c) Mouramora site (d) Padum Pukhuri; (e) Rukmini Garh, and (f) Pratima Garh.

2.2. XRD and FTIR Analysis

A small portion of the samples has been thoroughly grinded using an agate mortar to make a fine powder for XRD and FTIR analysis. The XRD analysis was carried out using the X-Ray diffractometer ULTIMA IV (Rigaku, Japan) with CuKα radiation in 2θ mode between 2° and 80° with ±2% basic accuracy. The mineral phases present in the studied bricks were identified after comparing their d-spacing and 2θ values in published literature (Chen, 1977; Lindholm, 1987; Tucker, 1988).

The FTIR spectra of the samples were determined after being pelletized with spectra grade KBr and recorded at room temperature in a wide range of wave numbers from 400 to 4000 cm^{-1} by using FTIR-SPECTRUM two (Perkin Elmer Inc.). The investigation of XRD and FTIR, analysis of the studied brick samples was performed at the CSIR-North East Institute of Science & Technology, Jorhat, India.

2.3. SEM and EDS Analysis

To understand the internal morphology of the brick samples, they were analysed using Scanning Electron Microscopy (SEM) and Energy Dispersive Spectrometer (EDS) techniques. The SEM coupled with the elemental analysis was done using Field Emission Scanning Electron Microscopy (FESEM) make in Carl ZEISS Microscopy, Germany. The samples coated with a thin layer of gold or platinum were examined with SEM, using various magnification for all the samples in the study. The investigation of SEM, and EDS analysis of the studied brick samples was performed at the CSIR-North East Institute of Science & Technology, Jorhat, India.

2.4. TL and OSL/IRSL Dating

For the TL and OSL/IRSL dating investigation, the material was sampled with a low-speed drill from the inner part of the bricks and all the procedures were followed under dim red light according to the fine-grain protocol (Zimmerman, 1971) the obtained polymineral fraction (4–11 μm) was deposited onto stainless steel discs and used for both TL and OSL/IRSL measurements. This fraction,

 doi:10.20944/preprints202406.0997.v1

mainly consisting in quartz and feldspars, can be excited by both blue (OSL) and infrared radiations (IRSL), the latter being effective only on feldspars.

TL/OSL/IRSL measurements were performed with a Risø TL-DA-20 reader, using blue-LEDs (470 ± 30 nm, ~72mW/cm^2) for OSL and infra-red LEDs (λ = 850 nm, ~270 mW/cm^2) for IRSL and detecting the emitted photons with an Electron Tube PDM 9107Q-AP-TTL-03 coupled with a U-340 filter for OSL and a Schott BG3/BG39 filter combination for IRSL measurements. The system is equipped with an internal ^{90}Sr-^{90}Y beta source (dose rate: 0.127 ± 0.05 Gy/s).

To evaluate the Equivalent Dose (E.D.), two different techniques were applied: the Multiple-Aliquot Additive protocol (MAAD, Aitken, 1985) was used with TL and the Single Aliquot Regenerative dose (SAR, Murray & Roberts, 1998) protocol with OSL and IRSL.

The annual dose rate was indirectly derived from the measurement of the radioactivity of the samples. The U and Th concentrations were obtained by total alpha counting using ZnS scintillator discs assuming a Th/U concentration ratio equal to 3.16 (Aitken, 1985). The contribution due to ^{40}K content was deduced from the total concentration of K obtained by flame photometry. For IRSL, the effect of the internal K-content of feldspar was considered. Alpha particles are less effective in inducing luminescence than beta and gamma radiation. This was considered by the a-value determination, which is based on the comparison of the luminescence signals induced by alpha and beta laboratory irradiations. Because water absorbed part of the radiation that would otherwise reach the sample, the saturation water content was evaluate for each brick. The F value (i.e. the fraction of saturation to which the assumed average water content corresponds) was considered equal (75 ±10) % for all samples, considering the available information of humidity of the area. The cosmic ray contribution to the final dose rate was added (Prescott & Hutton, 1994). The TL/OSL/IRSL dating have been performed in the LAMBDA Lab of Department of Material Science of the University of Milano-Bicocca, Milano, Italy (Panzeri et al., 2022).

3. Results and Discussion

In the following the obtained data are discussed.

3.1. Identification of Mineral through FTIR Analysis

The FTIR spectra of the studied brick samples are depicted in Figure 4 (a). Since a few FTIR spectra are not easy to recognize, the graphs have been separated into two ranges at 1200-400 cm^{-1} and 4000-3000 cm^{-1} (Figure 4 b and c). The minerals identified in the spectrum were based on existing literature sources (listed in Table 1). These minerals include quartz, feldspar (albite, orthoclase), kaolinite, palygorskite, chlorite, organic carbon, cerussite, hematite, and magnetite. All the brick samples under investigation contains quartz, kaolinite, organic carbon, and palygorskite (barring Rukmini Garh).

 doi:10.20944/preprints202406.0997.v1

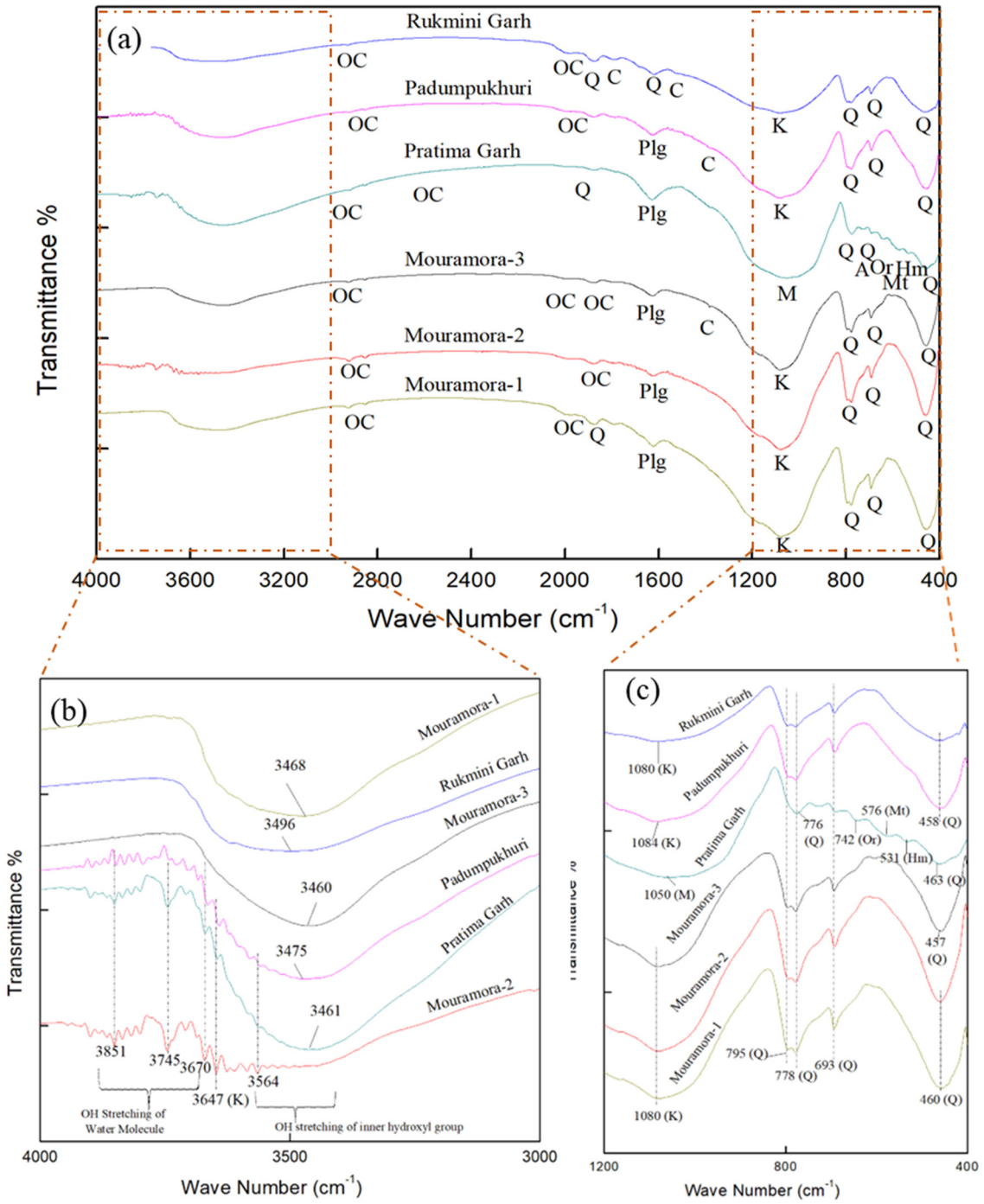

Figure 4. FTIR spectrum of studied brick samples (a) FTIR spectrum ranges from 4000-400 cm^{-1}, (b) FTIR spectrum ranges from 4000-3000 cm^{-1} and (c) FTIR spectrum ranges from 1200-400 cm^{-1} (Q-Quartz, Or-Orthoclase, A-Albite, Mt-Magnetite, Hm-Hematite, K-Kaolinite, Plg-Palygorskite, C-Carbonates, Ch-Chlorite, OC-Organic Carbon).

Table 1. FTIR spectra wave numbers with assign mineralogy of the studied brick samples.

Assigned mineralogy/Assignment	Frequency with relative Intensity (cm^{-1}) Sample No with absorption Frequency and relative Intensity (cm^{-1})						Reference
	MOURAMORA-1	MOURAMORA-2	MOURAMORA-3	PADUMPUKHURI	PRATIMA GARH	RUKMINI GARH	
Quartz	1870VW	-	-	-	1876VW	1873W	(Chutia et al., 2020; Hlavay et al., 1978; Keller & Pickett, 1949; V. Ramasamy et al., 2004, 2009)
	-	-	-	-	-	1619VW	
	-	795S	795S	-	-	-	
	778S	778S	778S	778S	776M	778SSp	
	693S	693M	694S	692M	693M	693S	
	460S	461S	-	-	463S	-	
	-	-	457S	458S	-	458S	
Microcline	-	-	-	-	1050S	-	(Theodosoglou et al., 2010)
Orthoclase	-	-	-	-	642W	-	(V. Ramasamy et al., 2009)
Albite	-	-	-	-	725W	-	(Legodi & De Waal, 2007) and references therein
OH Stretching of Water Molecule	-	3851VW	-	-	3851VW	-	
	-	3746VW	-	-	3745W	-	
	-	3671VW	-	-	-	-	
OH stretching of inner hydroxyl group	-	-	-	-	-	3496 WBr	(Elsass & Olivier, 1978; Bukalo et al., 2017; Govindasamy et al., 2019a; Seetha & Velraj, 2016)
	-	-	-	3475W	-	-	
	3468W	-	3460W	-	3462M	-	
Kaolinite	1080S	1080S	1081S	1084SBr	-	1081SBr	
	-	3647VW	-	-	-	-	
Chlorite	-	3565VW	-	-	-	-	(Jozanikohan & Abarghooei, 2022)
Palygorskite	1623W	1630W	1625W	1629W	1629W	-	(V. Ramasamy et al., 2009)
Carbonate Minerals	-	-	-	-	-	1788W	(Lyon, 1967; V. Ramasamy et al., 2009)
	-	-	1384W	1381VW	-	-	

doi:10.20944/preprints202406.0997.v1

Magnetite	-	-	-	-	576W	-	(Hindy et al., 2018)
Hematite	-	-	-	-	531W	-	(Chutia et al., 2020; V. Ramasamy et al., 2009)
Organic compound	2922VW	2922VW	2919VW	2919VW	2919VW	2928 VW	(Hindy et al., 2018; Libretexts, 2014; Raja Annamalai et al., 2014; V. Ramasamy et al., 2009; Shillito et al., 2009) Ramasamy 2009 and reference therein
	2851VW	2851VW	2854VW	2854VW	2854VW	-	
	-	-	-	-	2356VW	-	
	-	-	-	2004VW	-	-	
	1998VW	-	1998VW	-	-	1984 VW	
	-	1878VW	1879VW	1879VW	-	-	

Abbreviations: VW-Very weak, W-Weak, M-Medium, S-Strong, Br-Broad, SBr-Strong & broad, SSp-Strong & sharp, WBr-Weak & broad.

doi:10.20944/preprints202406.0997.v1

 doi:10.20944/preprints202406.0997.v1

The presence of quartz was confirmed by characteristic vibrational peaks at 457-458cm^{-1} (Si-O asymmetrical bending) and 460-463 cm^{-1}, (Si-O asymmetrical bending), 692-693 cm^{-1}(Si-O symmetrical bending), and 776-778 and 795 cm^{-1} (Si-O symmetrical stretching). The existence of quartz in the Mouramora-1, Pratima Garh, and Rukmini Garh brick samples has been supported by the presence of weak absorption peaks at 1619 cm^{-1} and 1870-1876 cm^{-1}.

The feldspar group of minerals is merely present in the Pratima Garh brick sample, which included orthoclase, microcline (K-feldspar), and albite (Na-feldspar). Their presence was established by vibrational peaks at 1050 cm^{-1}(Si-Al-O stretching for microcline feldspar), 642 cm^{-1} (Al-O coordination vibrations suggesting orthoclase feldspar), and 725 cm^{-1} (Al-O-Si stretching for albite feldspar).

In general, four significant IR spectra of OH-stretching regions are employed to distinguish kaolinite, with relative intensities of 3695, 3665, 3650, and 3620 cm^{-1} (Elsass and Olivier, 1978; Bukalo et al., 2017). However, the presence of other minerals may influence the intensity and resolution of these vibration bands. The studied samples encompass no prominent kaolinite peaks at 3695, 3665, 3650, or 3620 cm^{-1}. Bukalo et al., 2017assigned the OH stretching region peak with an intensity of 3647 cm^{-1} as kaolinite. In the presence of a peak at 3647 cm^{-1} with weak OH stretching of the inner hydroxyl group in the Mouramora-2 and Pratimagarh samples affirms the signatures of kaolinite. Other FTIR spectrum ranging from 3671-3851 cm^{-1} represents the OH stretching of water molecules. The 3460-3496 cm^{-1} spectra imply mixed layered OH stretching and bending vibrations inner-surface hydroxyl groups. The OH stretching of the inner hydroxyl group mineral chlorite was also observed in the Mouramora-2 samples at 3565 cm^{-1} regions. The IR spectrum for kaolinite with thin particles exhibits peaks at 1105 and 695 cm^{-1}, however as the particle size increased, the vibrational bands shifted to 1080 and 689 cm^{-1} (Elsass and Olivier, 1978). Barring the sample Padumpukhuri, rest of the five studied samples displays broadening bands at 1080 and 1084 cm^{-1}.

Carbonate minerals have been found in three different locations: Mouramora-3, Padum Pukhuri, and Rukmini Garh, with FTIR spectra of 1381, 1384, and 1788 cm^{-1}. The carbonate mineral with a prominent relative intensity at 1396 cm^{-1} resembles the mineral cerussite (Lyon, 1967). However, Ramasamy et. al (2009) considered the intensity ranges of 1380-1385 cm^{-1} as indicative mineral of cerussite. Hence, the presence of spectra at 1381, 1384 and 1788 cm^{-1} is in good agreement with the carbonate mineral cerussite and calcite, respectively.

The complex nature of absorption bands in stretching and bending regions of water molecules is a distinguishing feature of palygorskite. Palygorskite may be responsible for the presence of bands in the region 1623-1630 cm^{-1}. Many researchers have studied similar patterns (Hayashi et al., 1969; Russell, 1987; Serna et al., 1977).

An additional peak in the ranges 2919-2928, 2851-2854, 2004, 1984-1998, and 1878-1879 cm^{-1} indicates C-H stretching vibrations caused by a weaker organic compound (Bain & Fraser, 1994; Dios Cancela et al., 1996; Hajjaji et al., 2001; Song et al., 2001).

The prominent iron minerals hematite and magnetite were detected, with 531 and 576 cm^{-1} spectra in the Pratima Garh sample. Their presence was possibly due to replacement of Fe^{2+} and Fe^{3+} (Fysh & Fredericks, 1983).

3.2. Identification of Mineral through XRD Analysis

The XRD pattern of the studied brick samples has been presented in Figure 5. Non-clay minerals identified include quartz, feldspar (orthoclase, microcline, oligoclase, sanidine, and albite), aragonite, dolomite, laumontite, ilmenite, siderite, hematite, chlorite, trona, pyrite,magnesite, wollastonite, goethite, and glauconite. However, kaolinite minerals are not recorded in the XRD results, despite appearing in the FTIR, due to the disorderliness (loss of crystalline nature) of the respective minerals. The minerals with the most intense reflections are quartz (3.34Å), orthoclase (3.29Å, 3.31Å), and wollastonite (3.32Å). The clay mineral kaolinite is not identified in the XRD analysis, which may indicate that this mineral is completely disordered. Carbonate and iron-bearing minerals are noted.

 doi:10.20944/preprints202406.0997.v1

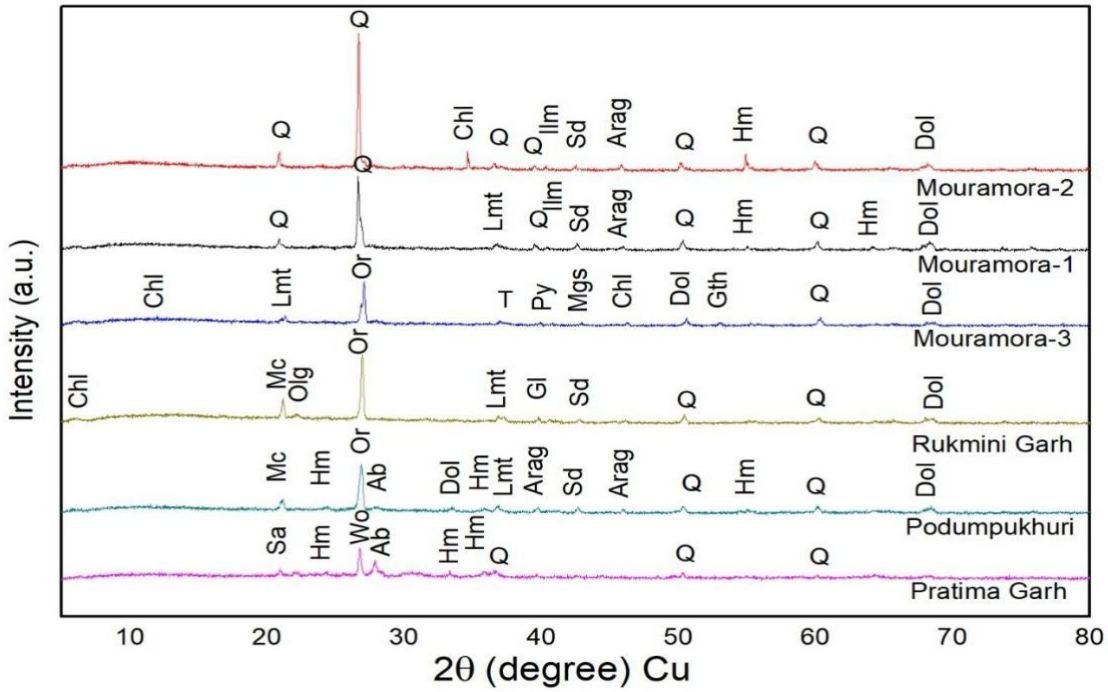

Figure 5. XRD pattern of studied brick samples (Q-Quartz, Feldspar (Or-Orthoclase, Mc-Microcline, Olg-Oligoclase, Sa-Sanidine, Ab-Albite), Arag-Aragonite, Dol-Dolomite, Lau-Laumontite, Ilm-Ilmenite, Sd-Siderite, Wo-Wollastonite, Hm-Hematite, Chl-Chlorite, T-Trona, Py-Pyrite, Mgs-Magnesite, Gth-Geothite, and Gl-Glauconite).

3.3. The Firing Temperature Analysis Using FTIR and XRD

The IR spectra of dioctahedral and trioctahedral layer silicates displays a very complex band system in the OH stretching region (Elsass & Olivier, 1978). In the present study, the absorption bands at 3671-3851 cm^{-1} and 3460-3496 cm^{-1} are assigned to the OH stretching of water molecules and OH stretching of the inner hydroxyl group, respectively and may corresponds to these complex stretching bands. However, upon heating of sample, it undergoes dehydration at 200°C and continues at 380°C, resulting in a weakening of the broad band of 3400cm^{-1} broad band and breaking of the crystal structure at 500°C (Elsass & Olivier, 1978). In addition, disorder in the octahedral and tetrahedral sheets is notable, with partial removal of the 535 cm^{-1} Si-O bending band and broadening of the Si-O stretching bands in the 1100-1000 cm^{-1} region (Elsass & Olivier, 1978). The broadening of Si-O stretching bands at 1100-1000 cm^{-1} region in the studied bricks implies a firing temperature of 500°C. Additionally, at 500°C, the absorption peak at 915 cm^{-1} indicates that Al (OH) vibrations in an octahedral sheet structure begin to collapse (Elsass & Olivier, 1978; Maniatis et al., 1982; Miller, 1961; Raja Annamalai et al., 2014; K. Ramasamy & Kamalakkannan, 1987). The absence of 915cm^{-1} spectra in the studied samples suggests that all the samples were fired above 500°C.

With increasing temperature, the Si-O stretching band shifts towards higher frequencies and broadens, with the maximum intensity around 1025 cm^{-1} at 100°C and shifting to the band around 1036 cm^{-1} at 600°C (Damjanović et al., 2011; Raja Annamalai et al., 2014). The silicate structure disappeared when the clay was fired to 650°C, and a broad symmetry band was detected at 1035 cm^{-1} for red clay and 1080 cm^{-1} for white clay (Maniatis & Tite, 1981; Raja Annamalai et al., 2014). The presence of an absorption band in five samples around 1080-1084cm^{-1} indicates that white clay of kaolinitic composition was used in the investigated brick samples, which were fired to 650°C.

The presence of hematite and magnetite, as indicated by the peak at 540 cm^{-1}, is an indication of iron oxides formed during fabrication firing processes above 650°C (Raja Annamalai et al., 2014; Ravisankar et al., 2012, 2013). However, the presence of hematite implies that they were fired in open air or in a completely oxidising atmosphere at the time of manufacture (Ravisankar, Kiruba,

 doi:10.20944/preprints202406.0997.v1

Naseerutheen, et al., 2011; Ravisankar, Kiruba, Shamira, et al., 2011). The presence of hematite and magnetite in the studied Pratima Garh sample indicates that it was fired above 650°C in open air or in a perfectly oxidising atmosphere at the time of manufacture, and the type of clay used is plausibly red clay. It can also be inferred that the artisans of Pratima Garh brick were well aware of the technology implemented in firing the bricks under both an oxidizing and a reduced atmosphere, which is inferred by the presence of peaks of 531 and 576 cm^{-1} respectively.

During the firing of clay resembles remarkable changes at 1000 to 1200 °C, where the X-ray diffractogram of quartz become disappears. Gradually quartz decomposes from 800 to 1100°C, peaking at 1100°C and then disappearing. Up to 800°C, all the decomposed and disappearing phases contribute to the formation of a vitreous phase. At this point, the clay would be mostly amorphous, with some residual grains of quartz, neo formed mullite, hematite and other high-temperature mineral phases like microcline. As a result, except at 1200°C, quartz was a residual phase, i.e., a component of the raw clay that did not undergo chemical transformations during the firing stage. On the contrary, during the firing process, mullite, hematite and other silicates were formed. At temperatures ranging from 700 to 900°C, clays showed phyllosilicate destruction followed by vitrification, which is significant at temperatures above 1000°C (Castellanos et al., 2012).The presence of orthoclase, microcline, albite, hematite, and magnetite in the Pratima Garh, Rukmini Garh, Padumpukhuri and Mouramora- bricks supports the high firing temperature of more than 800°C.

Clay deposits typically contain some organic material, but artisans can also add organic compounds to the ceramic paste during the preparation process to increase plasticity (Shoval, 1994).

At ~400-650 °C, depending on the type of flux and other raw materials used, the initial ingredients decompose and CO_2, S, and hydrocarbons are lost. Dehydration occurs at ~100°C, followed by dehydroxylation of clay minerals at temperatures ranging from ~450 to 750°C, depending on the type and purity of the clay (Russ et al., 2005). Dehydration and dehydroxylation of relatively pure clay minerals occur at various temperatures depending on the clay minerals present. Chlorite loses water at a relatively high temperature, usually starting at ~750, but this temperature is determined by the mineral chemistry. Illite (mica) transformation begins with dehydration at ~600-700°C. When carbonate minerals are heated, they release carbon dioxide; for example, calcite decomposition begins at 650°C. The temperature of phase transformation varies from sample to sample due to a variety of factors such as mineral grain size, heating rate, and how easily the evolved carbon dioxide can be lost to the atmosphere (Cultrone et al., 2004). At ~573°C, alpha/low quartz structurally transforms into beta/high quartz. Because this transition involves rotation rather than bond breaking, the reaction is reversible, and any high-quality quartz that remains after the high-temperature soak will invert to low-quality quartz during the cooling phase of the firing cycle. The brick expands as the temperature rises; however, if the cooling rate is too fast, highly damaging microcracking can occur (Grim, 1968).

The firing minerals that are generated during the production of pottery are dependent on a number of factors, including the makeup of the clay, materials added to it, the atmosphere, and the length of the firing process. High-temperature minerals such as gehlenite and diopside are formed from the decomposition products of illite and calcite (Maritan et al., 2006; İssi et al., 2011; Papachristodoulou et al., 2006). At 650°C, calcite starts to break down; at 850°C, high-temperature calco-silicates and alumino-calco-silicates, such as diopside and anorthite, are the products of this process. At temperatures higher than 830°C, wollastonite—which is created when quartz and lime react at approximately 920 to 1000°C—replaces gehlenite in systems that contain gehlenite (Böhme et al., 2019). The presence of wollastonite and feldspar (albite, orthoclase, and microcline) in the Pratima Garh, Padumpukhuri, Rukmini Garh and Mouramora-3 brick samples indicates that the bricks were fired at temperatures above ~800°C. The presence of the iron oxide minerals hematite and magnetite in the same sample, on the other hand, indicates that they were fired at temperatures higher than 650°C, as indicated by the FTIR and XRD studies. In their analytical study of ancient pottery, discovered that feldspar decomposes at temperatures ranging from 900 to 950°C (Iordanidis et al., 2009). The presence of feldspar in the samples indicates that they were all fired at temperatures lower than 900°C. This clearly shows that the Pratima Garh, Padumpukhuri, Rukmini Garh, and

 doi:10.20944/preprints202406.0997.v1

Mouramora-3 brick samples were fired at temperatures lower than 900°C in oxidising kiln atmospheric conditions. The estimated firing temperature of the samples is presented in Table 2. However, research concentrating on Thermogravimetry-Differential Thermal Analysis (TG-DTA), apparent porosity, water absorption, and other pertinent aspects will be required to establish the accurate fire temperature of the investigated bricks.

Table 2. Estimation of firing temperature of studied brick samples based on FTIR and XRD analysis.

S.No.	Sample ID	Colour	Type of the Clay	Estimation of firing temperature
1	Mouramora-1	Light red colour	White clay	Below 650ºC
2	Mouramora-2	Light red colour	White clay	Below 650ºC
3	Mouramora-3	Light red colour	White clay	Above ~ 800ºC
4	Padum Pukhuri	Light red	White clay	Above ~ 800ºC
5	Rukmini Garh	Reddish yellow	White clay	Above ~ 800ºC
6	Pratima Garh	Weak red	Red clay	Above ~ 800ºC

3.4. The Firing Temperature Analysis Using and SEM-EDS

SEM-EDS provides valuable information on the pore structure and the glassy phase development used to study systematically the internal morphology changes occurring when fired in a temperature range 600°C to 1300°C and this can be employed and coupled with Energy Dispersive spectrometer (EDS) for minerals detection (Maniatis et al., 1983). Scanning Electron Microscope is a vital tools to examine ancient pottery and established the ancient ceramic technology (Tite & Maniatis, 1975). It is an excellent tool and it has been found useful in many applications to characterize the archaeological artifacts (Goldstein et al., 2003; Tite, 1992). The SEM with EDS analysis is non-destructive and capable of offering precise elemental composition information towards the analysis of archaeological potsherds. They conclude that the presence of Ca as tine grained and evenly distributed calcite in clays significantly affects the development of vitrification, if calcium present in the sample, say $CaCO_3$, dissociates into CaO and vitrification sets in around 850°C.

The non-calcareous clays fired at temperatures below 800°C will produce no vitrification (Maniatis & Tite, 1978). However, well- crystallized hematite is abundant in non-calcareous clays. The absence in the studied bricks of vitrification, is the evidence of firing temperature below 800°C during manufacturing by artisans and it is well evidenced by FTIR, and XRD study. Firing at 900°C produces much more pronounced changes in the clay body, sintering is quite advanced and much vitrification has been produced (Maniatis et al., 1983). (Leriche et al., 2017) Leriche et al. 2017, stated

 doi:10.20944/preprints202406.0997.v1

that continuous heating initiates densification which leading to a reduction in porosity and later it could lead to the generation of residual porosity and initial grain growth. They also opined that this process initially creates necks between particles, followed by developments of cylindrical shape interconnected pores and lastly pores change to a more spherical and isolated state as temperature increases. The SEM micrographs of the studied samples show the micropores are cylindrical shape with interconnected pores (Figure 6a & b). as well as change in pores shape to spherical and isolated state (Figure 6c-f) suggests that the heating temperature increases in the bricks of Mouramora-3, Padum Pukhuri, Pratima Garh, and Rukmini Garh, then the Mouramora-1 and Mouramora-2 bricks.

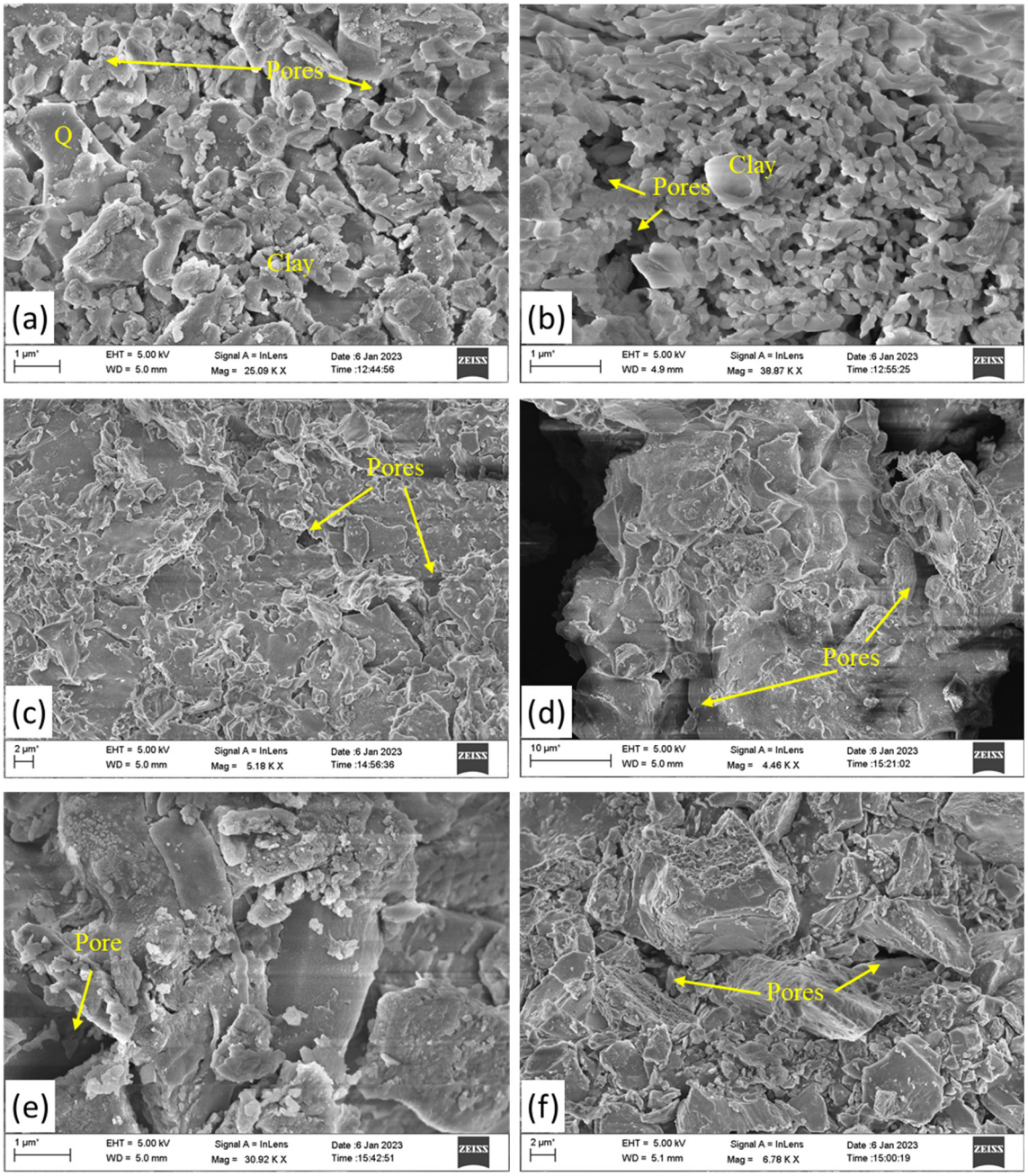

Figure 6. Representative SEM backscattered image of surface morphology of studied fired brick samples, (a) Mouramora-1, (b) Mouramora-2, (c) Mouramora-3, (d) PadumPukhuri, (e) Pratima Garh, (f) Rukmini Garh.

The chemical composition of the sample was obtained by EDS analysis and its representative spectrum is shown in Fig 7. From the EDS analysis, the potsherds mainly have the concentrations of silica (SiO_2), alumina (Al_2O_3) and fluxes (Na_2O, K_2O, Fe_2O_3, CaO, MgO and TiO_2) as the compositions were identified in all the samples except Na_2O, CaO and TiO_2 in Padum Pukhuri, CaO and TiO_2 in

 doi:10.20944/preprints202406.0997.v1

Mouramora 1 and CaO in Mouramora 2. Researchers claim that the total flux concentration within potsherds provides valuable insights into the thermal behaviour of bricks, contributing to the formation of a vitreous or glassy phase (Lecomte et al., 2004; Osborn & Muan, 1960). When multiple components like Na_2O, TiO_2, Fe_2O_3, CaO, and MgO, are present along with SiO_2 and Al_2O_3, a large portion of liquid is generated which is referred to as glassy or vitreous phase (Garzón et al., 2022). The total flux content of potsherds was determined using the formula Total Flux Content = RO + R_2O + Fe_2O_3 + TiO_2, where RO = CaO + MgO and R_2O = K_2O + Na_2O (Garzón et al., 2022; Sánchez-Soto et al., 2023). In the present study the total flux content has been calculated, which values ranges 8.91–25.77 wt%, where samples from Mouramora-3, Padum Pukhuri, Pratima Garh, and Rukmini Garh exhibited higher values, whereas Mouramora-1 and Mouramora-2 bricks displayed lower values.

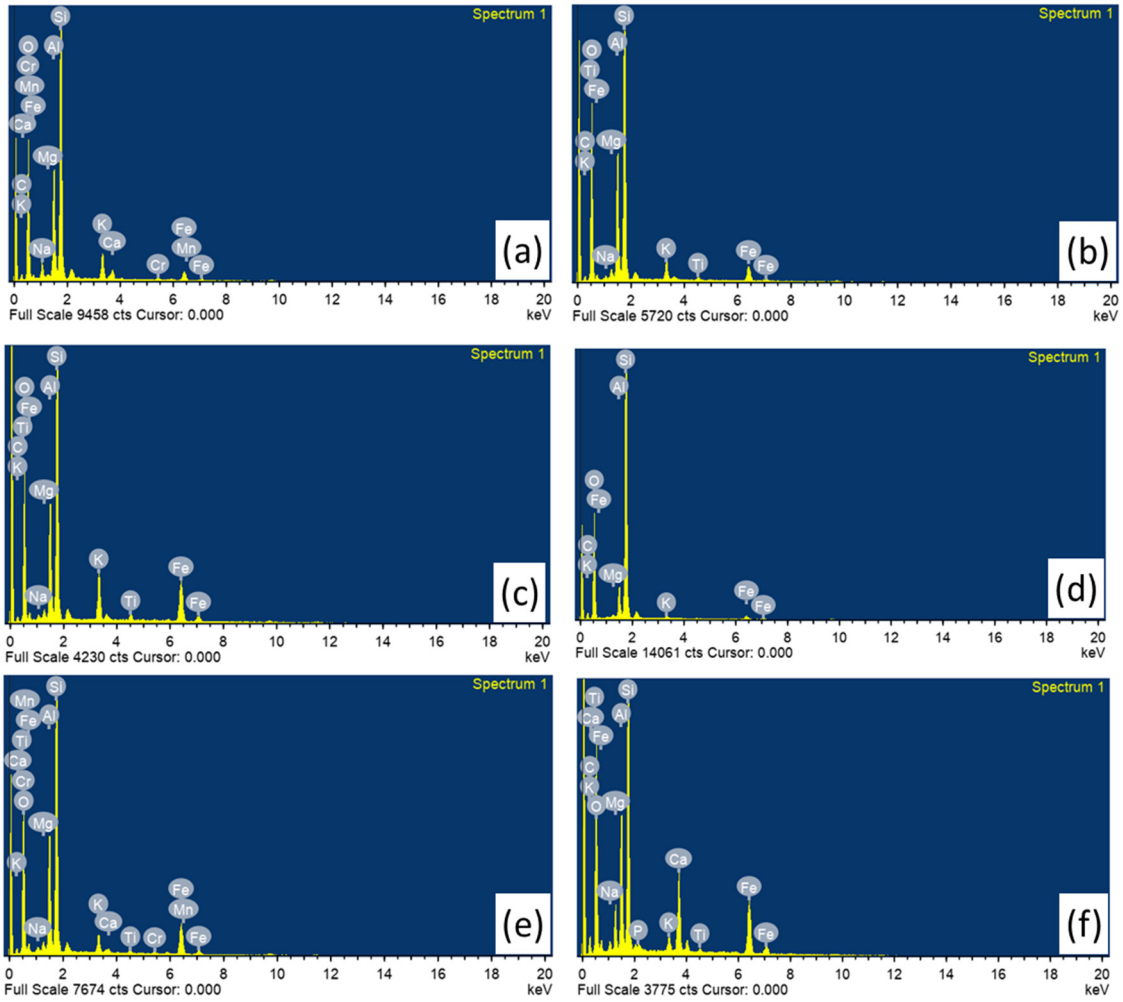

Figure 7. Representative EDS pattern of studied fired brick samples, (a-c) Mouramora-1; Mouramora-2 and Mouramora-3 respectively, (d) PadumPukhuri; (e) Rukmini Garh and; (f) Pratima Garh.

If the fluxes concentration (K_2O, Fe_2O_3, CaO, MgO and TiO_2) are more than 9% the clays are classified as low refractory and classified as high refractory if the fluxes in the sample are less than 9% (Ravisankar et al., 2013). On the other hand the clays containing CaO greater than 6%, are known as Calcareous clays and CaO less than 6% are known as non-calcareous clays (Maniatis & Tite, 1981). Based on the above statement and from EDS results it is inferred that the baring Pratima Garh bricks all the studied samples have been made of non-calcareous clay. Moreover Mouramora-1, Mouramora-2 and Padum Pukhuri show high refractory clay and Mouramora-3, Pratima Garh and Rukmini Garh reflect low refractory characteristics. From the analysis, silica is enriched in all the samples and found as the major element in all the bricks percentage varies from 66.81% to 82.10%. All the bricks having low refractory clay consists high Iron oxide content ranges from 10.88% to

 doi:10.20944/preprints202406.0997.v1

12.84%. The chromium concentrations have been noticed in two of the studied samples Mouramora-1 (0.53%) and Rukmini Garh (0.47%). It should be noted, however, that the pottery composition depends both in the clay source and in the recipe used to prepare the clay paste (Papachristodoulou et al., 2006). The variation of chemical composition of bricks may imply pottery from different production sites or reflect the natural inhomogeneity of local clay deposits and the application of different manufacture processes in local workshops. The SEM-EDS result for the firing temperature analysis is in good agreement with the FT-IR, and XRD results.

3.5. TL, OSL and IRSL Results

TL, OSL and IRSL equivalent doses (E.D.) were evaluated for all samples; because no mineralogical phase separation has been performed on the brick samples, any luminescent mineral contributes to the emission, quartz and feldspars being the main emitters. Both quartz and feldspars have a TL emission in the blue region of the spectrum and their contribution is not separate. For what concerns OSL, while the blue light stimulates the emission of both quartz and feldspars, IR-light only stimulates that of feldspars, for this very reason both OSL and IRSL has been performed. Typical examples of TL glow curves are shown in Figure 8a. Based on the plateau test, that allows to identify the thermally stable portion of the curves (Aitken, 1985), the TL signals were integrated between 300 and 350 °C. Plotting the intensity of the TL signal vs. the laboratory imparted dose, E.D. was extrapolated by linear regression, as illustrated in Figure 8b. The results of such evaluations are summarized in Table 3.

Table 3. Saturation water contents (W), a-values, U, Th and K_2O concentrations. E.D., dose rates for quartz and feldspars, ages, dates and errors obtained with different luminescence technique on brick samples.

SAMPLE ID	W (%)	a value	ppm U (± 5%)	ppm Th (± 5%)	K_2O (± 3%)	E.D. (Gy)	Dose rate (mGy/a)	Age (y)	Date	Error
Mour1 TL	18	0.14	4.1	12.9	2.98	2.2 ± 0.3	6.9 ± 0.3	320	1700	60
Mour-1 IRSL	18	0.14	4.1	12.9	2.98	2.6 ± 0.8	7.5 ± 0.3	350	1670	90
Mour-2 TL	23	0.18	4.3	13.8	2.56	2.7 ± 0.3	7.2 ± 0.4	380	1640	60
Mour-2 IRSL	23	0.18	4.3	13.8	2.56	3.1 ± 0.5	7.8 ± 0.4	400	1620	90
Mour-3 TL	24	0.14	4.2	13.4	3.52	2.7 ± 0.3	7.6 ± 0.4	360	1640	70
Mour-3 IRSL	24	0.14	4.2	13.4	3.52	1.8 ± 0.2	7.7 ± 0.4	230	1790	60
Rukmini										
Prat TL	33	0.14	5.0	15.8	3.52	3.6 ± 0.3	7.3 ± 0.4	490	1530	60
Prat IRSL	33	0.14	5.0	15.8	3.52	4.2 ± 0.3	7.9 ± 0.4	530	1490	70
PadumTL	30	0.25	2.7	8.5	1.48	4.9 ± 0.4	4.9 ± 0.2	1000	1020	120

 doi:10.20944/preprints202406.0997.v1

PadumOSL	30	0.25	2.7	8.5	1.48	4.2 ± 1.0	4.9 ± 0.2	860	1160	250
PadumIRSL	30	0.25	2.7	8.5	1.48	1.6 ± 02	5.5 ± 0.2	290	1730	60

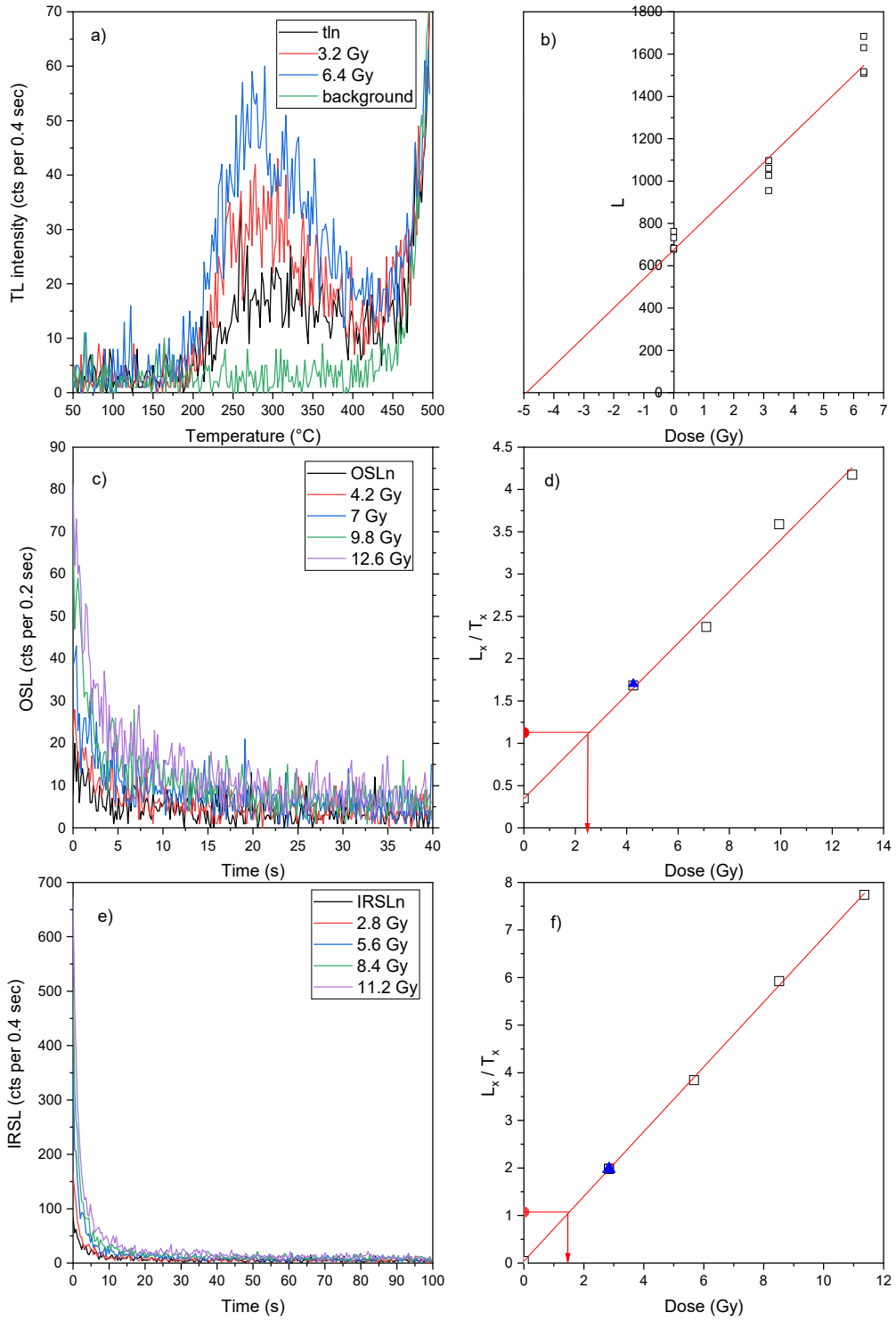

Figure 8. a) TL glow curves, c) OSL and e) IRSL shine down curves f Padum Pukhuri sample.b) Growth curve of the TL signal with imparted additive dose. TL glow-curves were integrated between 300-3500°C and the signal of the background in the same temperature interval (green line) was subtracted. Sensitivity corrected d) OSL and f) IRSL response to a fixed dose vs the laboratory

 doi:10.20944/preprints202406.0997.v1

imparted regenerative dose. The red dot is the natural signal and the blue triangle is the recycling ratio point.

Typical OSL/IRSL shine-down curves are shown in Figure 8c-e. The samples were stimulated for 40 s in case of OSL measurement and 100 s for IRSL. The preheat temperature was 200°C for 10 while the cut-heat was 180°C and it was chosen using a preheat plateau test. For the E.D. determination, the initial part of the OSL/IRSL decay curve was used, specifically the first 0.6 s for OSL and the first 1.6 s for IRSL. The background was assumed as the average signal of the last 10s (OSL) or 20s (IRSL) of stimulation. Plotting the intensity of the OSL/IRSL signal vs. the laboratory imparted dose, E.D. was determined by interpolation of the natural signal on the linear regression, as illustrated in Figure 8d and 8f.

In general, it can be said that the luminescence signals of the samples are rather weak, especially as regards the OSL signal. For this reason, it was possible to use this technique only to date the Padum Pukhuri sample, whose OSL curves have a sufficiently high intensity. IRSL, on the other hand, is the technique that gave the most intense signals for all samples.

By looking at the dating results obtained with TL, OSL and IRSL (Table 3), it is possible to observe that the low luminescence intensity of the samples caused high errors in the ages obtained. The results obtained with TL are in good agreement with those obtained with IRSL, except for the Padum Pukhuri sample. For the latter sample there is instead a good agreement between the ages obtained with TL and OSL.

It is well-known that minerals like feldspars can give underestimated ages for the presence of anomalous fading (Wintle, 1973), a malign phenomenon due to the loss of charge from thermally stable defect sites via non-thermal mechanisms. A specific fading test was therefore performed at room temperature for one months and a significant loss of signal has been observed, as shown in Figure 9 for the Padum Pukhuri sample. Therefore, fading evaluations were performed on all samples for all the luminescence technique used (TL, IRSL and OSL). For each sample and for each type of luminescence the g-values (Huntley & Lamothe, 2001) were determined (see Table 4). The ages of the samples obtained were then recalculated according to the equation of (Huntley & Lamothe, 2001) to obtain the dates corrected for the fading phenomenon (Table 4).

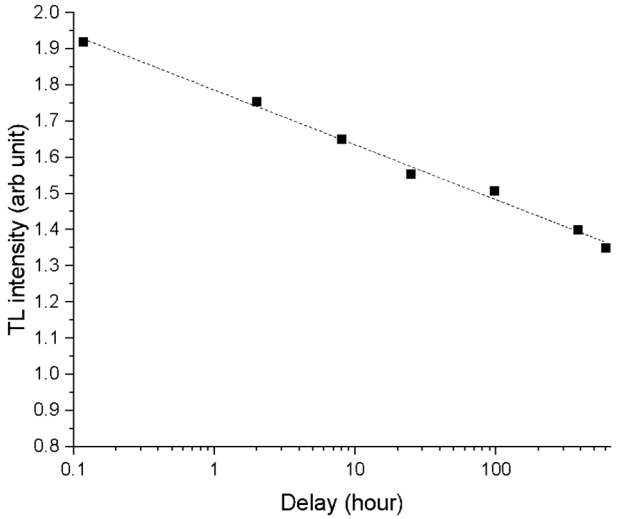

Figure 9. Anomalous fading TL data obtained on Padumpukhuri sample. Seven samples were irradiated with a dose of 6.4 Gy. A sample was measured immediately after irradiation while the others were kept in the dark for periods ranging from one hour to a month.

The high g-values (> 7%) obtained for nearly all the samples suggest the presence of some luminescent mineralogical phase other than feldspars with a high fading rate. In literature (Garcia

 doi:10.20944/preprints202406.0997.v1

Guinea et al., 1999) reported a TL emission of kaolinite in the blue region of the spectrum. Ten years later it was found that this mineral could be potentially valid for dosimetric purposes since it is sensitive to radiation and possesses a good dose linearity in the range of 50mGy to 8 Gy (Correcher et al., 2010). However, the stability of the TL signal during six months of storage shows an initial rapid decay (ca. 60%) followed by a mild slope reaching the stability after six months. Moreover, this mineral stands as very promising candidates towards IRSL dating, based on the very good IRSL response of this material to artificial beta irradiation (Polymeris et al., 2013).

Based on these results and on data obtained by FTIR and XRD analyses that confirm the presence of kaolinite in all the bricks studied, the dosimetric properties of kaolinite were more deeply investigated. Hence, the TL, OSL and IRSL measurements were carried out on a kaolinite coming from Monte Bracco (Barge, CN, Italy). The sample present luminescence signal either when heated or when illuminated with blue and IR light; Figure 10 shows TL, OSL and IRSL signals when irradiated with dose from 9 to 92 Gy. There is a linear growth of signal with dose in TL (at least up to 92 Gy), OSL and IRSL (up to about 37 Gy). At this point the stability of the TL, OSL and IRSL signals of kaolinite were investigated. A fading test was performed and it was noted that the measured luminescence signal (TL, OSL and IRSL) decreases as the time between irradiation and measurement increases (Figure 11). Unfortunately, it was not possible to determine the g-value for any of the luminescence techniques used as the decay of the luminescence signals does not follow the exponential decay law used for feldspars. The significant loss of luminescent signal over time, however, allows us to identify kaolinite as a possible cause of the high g-values obtained on the bricks analyzed in this work.

Table 4. g-values, ages and dates corrected for anomalous fading.

SAMPLE ID	g-value	Age faded	Date faded
Mour1 (TL)	6.8 ± 0.4	630 ± 130	1390 ± 130
Mour-1 (IRSL)	7.9 ± 0.5	920 ± 220	1100 ± 220
Mour-2 (TL)	8.4 ± 1.8	1010 ± 300	1010 ± 270
Mour-2 (IRSL)	5.7 ± 1.5	870 ± 250	1150 ± 250
Mour-3 (TL)	9.0 ± 0.3	1170 ± 280	850 ± 280
Mour-3 (IRSL)	9.8 ± 0.3	910 ± 250	1110 ± 250
Prat (TL)	8.6 ± 2.1	1410 ± 390	610 ± 390
Prat (IRSL)	9.0 ± 0.2	1860 ± 300	160 ± 500
Padum (TL)	3.4 ± 0.7	1350 ± 180	670± 180
Padum (OSL)	3.3 ± 0.6	1140 ± 360	880 ± 360
Padum (IRSL)	9.1± 0.1	1040 ± 200	980 ± 200

Preprints.org (www.preprints.org) | NOT PEER-REVIEWED | Posted: 14 June 2024 doi:10.20944/preprints202406.0997.v1

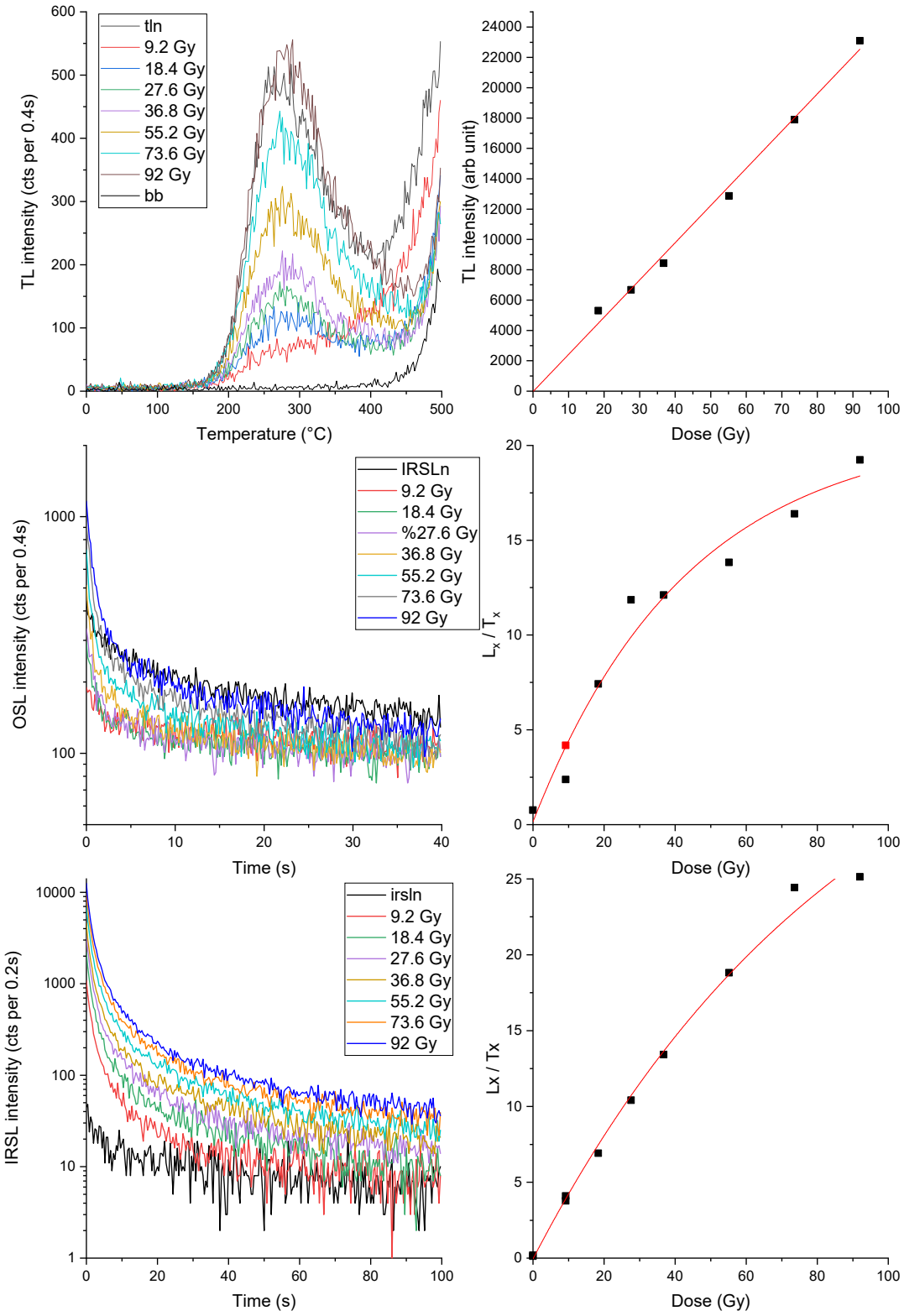

Figure 10. Luminescence signals of kaolinite. a) TL glow curves and b) corresponding growth of TL signal with dose; c) OSL shine-down curves and d) corresponding growth of OSL signal with dose; e) IRSL shine-down curves and f) corresponding growth of IRSL signal with dose.

 doi:10.20944/preprints202406.0997.v1

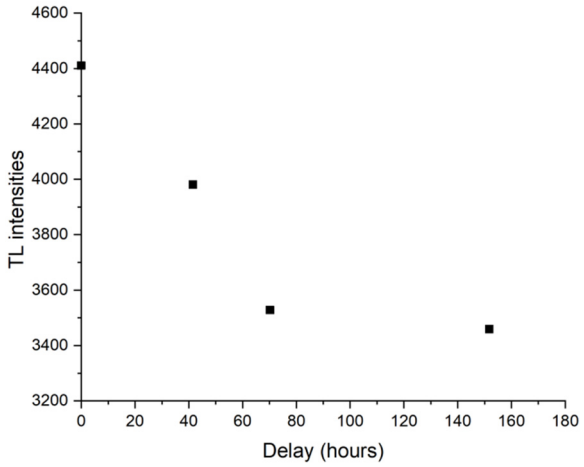

Figure 11. Anomalous fading TL data obtained on kaolinite. The sample was irradiated with 92 Gy and the TL signal was measured. A test dose equal to 10Gy was then imparted on the same aliquot and used to normalize the signal in order to consider the sensitization of the sample between the different irradiation and measurement cycles. At this point the same aliquot was irradiated again with 792Gy and stored in the dark for a certain time after which the TL curve and the related test dose were recorded.

3.6. Chronology of Bricks

The mineralogical characterisation and chronology of the present study infers the existence of two distinct group with technology having different firing temperature. One below 650ºC resembling XI-XIV centuries CE on the South Bank of the River Brahmaputra and other above 650ºC up to 830 ºC resembling VII-X centuries CE (Table-5) on the North Bank of the River Brahmaputra. These two divisions could indicate two different civilizations with technologies that permit to fire the bricks in different oxidizing kiln atmospheric conditions. From the present investigation it can be summarized that the first group of people were lived during VII-X centuries CE which were technologically sound and their state boundaries might be limited to northern bank of Brahmaputra as well as foothills of Arunachal Pradesh (studied bricks were from Padum Pukhuri, Pratima Garh and Rukmini Garh). The second group of people were lived during XI-XIV centuries CE which were technologically less sound then the first group and their state boundaries might be confined to the southern bank of the river Brahmaputra. Sheikh (Sheikh, 2017) performed dating of bricks from Kamakhya Temple of Assam, India suggesting two distinct age ranges as 500 CE and 800 CE. He opined that some segment of the existing Kamakhya temple might have been reconstructed later in 800 CE, which bricks production technology was more sound then the earlier inhabitant. Hence, it can be assumed that the bricks found from northern bank of Brahmaputra as well as foothills of Arunachal Pradesh (Padum Pukhuri, Pratima Garh and Rukmini Garh) along with those bricks from Kamakhya Temple dating to 800 CE were probably manufactured by a similar group of people residing in that time.

It is relevant to remember, dating the bulk material of construction bricks can mislead from the correct age, since the dated event corresponds to the last heating (> 500 °C) of the material, generally related to the brick production, that can be significantly different from that of the construction, also due to the practice of reuse of old bricks. But it is noteworthy that the cause of technological changes between the two group might be a scope for the further research.

The use of production material like calcareous and non-calcareous clay having low and high refractory nature for making bricks also infers that the bricks may produce in different production sites or reflect the natural inhomogeneity of local clay deposits and the application of different manufacture processes in local workshops.

 doi:10.20944/preprints202406.0997.v1

Table 5. Estimated ages, firing temperature and type of clay used in the studied archaeological sites.

Name of Archaeological sites	Type of Clay used	Calculated Age	Estimated Firing Temperature
Mouramora-1	Non-calcareous		Below 650ºC
Mouramora-2	Non-calcareous	XI-XIV sec CE	Below 650ºC
Mouramora-3	Non-calcareous		Above ~800 ºC
Pratima Garh	Calcareous	VII-X sec CE (i.e.,	Above ~800 ºC
PadumPukhuri	Non-calcareous	pre-Ahom)	Above ~800 ºC
Rukmini Garh	Non-calcareous	Not datable	Above ~800 ºC

4. Conclusions

From the integrated use of different spectroscopic techniques as FTIR, XRD, SEM -EDS and absolute dating methodologies chronology (TL, OSL, IRSL) it can be concluding that the studied archaeological site records existence of two distinct stratified group of people. They produced bricks in different oxidizing kiln atmospheric conditions. The chronological data infer that the first group of inhabitants (i.e., 700 ~1000 years back) have used more advanced technologies to fire the bricks (i.e., above 800 ºC) as verified for the sample Pratima Garh and PadumPukhuri.

The second group of inhabitants (i.e., 1100 ~1400 years back) have used technologies lower than the previous inhabitants having the ability to fire the bricks below 650ºC, as verified for the Mouramora samples.

Declaration of Competing Interest: All authors declare that they have no conflicts of interest.

Acknowledgments: At the very outset we extend our sincere gratitude to the Indian National Science Academy (INSA) for providing us financial assistance to conduct the project (Sanction No: HS/RC/300). Further, we are deeply thankful to the CSIR-North East Institute of Science & Technology, Jorhat, India, for providing the necessary facilities for the SEM-EDS, XRD and FTIR analysis of the studied brick samples. We also gratefully acknowledge the Directorate of Archaeology, Government of Assam, India, for providing us the permission to collect samples from Archaeological sites.

References

1. Aitken, M. J. (1985). *Thermoluminescence dating*. Academic Press. https://cir.nii.ac.jp/crid/1130282271912805376
2. Aitken, M. J. (1998). An introduction to Optical Dating: The Dating of Quaternary Sediments by the Use of Photon-Stimulated Luminescence. Oxford Science Publications.
3. Bain, D. C., & Fraser, A. R. (1994). An Unusually Interlayered Clay Mineral from the Eluvial Horizon of a Humus-Iron Podzol. *Clay Minerals*, *29*(1), 69–76. https://doi.org/10.1180/claymin.1994.029.1.08
4. Böhme, N., Hauke, K., Neuroth, M., & Geisler, T. (2019). In situ Raman imaging of high-temperature solid-state reactions in the CaSO4–SiO2 system. *International Journal of Coal Science & Technology*, *6*(2), 247–259. https://doi.org/10.1007/s40789-019-0252-7
5. Bukalo, N. N., Ekosse, G.-I. E., Odiyo, J. O., & Ogola, J. S. (2017). Fourier Transform Infrared Spectroscopy of Clay Size Fraction of Cretaceous-Tertiary Kaolins in the Douala Sub-Basin, Cameroon. *Open Geosciences*, *9*(1), 407–418. https://doi.org/10.1515/geo-2017-0031
6. Castellanos, A. O. M., Río, R. C. A., Ramos, G. M. A., & Plaza, P. E. V. (2012). A comparative study of mineralogical transformations in fired clays from the Laboyos Valley Upper Magdalena Basin (Colombia). 34(1), 43–55.
7. Chen, P.-Y. (1977). Table of key lines in X-ray powder diffraction patterns of minerals in clays and associated rocks. https://igws.indiana.edu/bookstore/details.cfm?Pub_Num=OP21
8. Chutia, A., Taye, C. D., Daimari, J., & Chutia, D. (2020). Petrography and Clay Mineralogical Study of the Siwalik Group of Rocks Exposed along Pasighat-Mariyang Road Section, East Siang District, Arunachal

Pradesh, Northeast India. *Journal of the Geological Society of India*, *95*(3), 263–272. https://doi.org/10.1007/s12594-020-1424-1

9. Correcher, V., Garcia-Guinea, J., Crespo-Feo, E., Rodriguez-Lazcano, Y., & Prado-Herrero, P. (2010). Dose–response of thermoluminescence in natural kaolinite. *Thermochimica Acta*, *503–504*, 12–15. https://doi.org/10.1016/j.tca.2010.02.013
10. Cultrone, G., Sebastián, E., Elert, K., De La Torre, M. J., Cazalla, O., & Rodriguez–Navarro, C. (2004). Influence of mineralogy and firing temperature on the porosity of bricks. *Journal of the European Ceramic Society*, *24*(3), 547–564. https://doi.org/10.1016/S0955-2219(03)00249-8
11. Damjanović, L., Holclajtner-Antunović, I., Mioč, U. B., Bikić, V., Milovanović, D., & Evans, I. R. (2011). Archaeometric study of medieval pottery excavated at Stari (Old) Ras, Serbia. *Journal of Archaeological Science*, *38*(4), 818–828. https://doi.org/10.1016/j.jas.2010.11.004
12. Dhanapandian, S., Shanthi, M., & Manoharan, C. (2010). FTIR and Mossbauer Studies on Industrial Clay Bricks from Three Different Regions of Tamilnadu State, India. 4, 122–126.
13. Dios Cancela, G., Romero Taboada, E., Huertas, F. J., Hernández Laguna, A., & Sánchez Rasero, F. (1996). Interaction of Trialkyl Phosphites with Montmorillonites. *Clays and Clay Minerals*, *44*(2), 170–180. https://doi.org/10.1346/CCMN.1996.0440202
14. Elsass, F., & Olivier, D. (1978). Infra-red and electron spin resonance studies of clays representative of the sedimentary evolution of the basin of Autun. *Clay Min. 13 (3)*, 299-308.
15. Fernandes, F. M., Lourenço, P. B., & Castro, F. (2010). Ancient Clay Bricks: Manufacture and Properties. In M. B. Dan, R. Přikryl, & Á. Török (Eds.), *Materials, Technologies and Practice in Historic Heritage Structures* (pp. 29–48). Springer Netherlands. https://doi.org/10.1007/978-90-481-2684-2_3
16. Fysh, S. A., & Fredericks, P. M. (1983). Fourier Transform Infrared Studies of Aluminous Goethites and Hematites. *Clays and Clay Minerals*, *31*(5), 377–382. https://doi.org/10.1346/CCMN.1983.0310507
17. Galli, A., Martini, M., Montanari, C., Panzeri, L., & Sibilia, E. (2006). TL of fine-grain samples from quartz-rich archaeological ceramics: Dosimetry using the 110 and TL peaks. *Radiation Measurements*, *41*(7–8), 1009–1014. https://doi.org/10.1016/j.radmeas.2006.06.011
18. Galli, A., Sibilia, E., & Martini, M. (2020). Ceramic chronology by luminescence dating: How and when it is possible to date ceramic artefacts. *Archaeological and Anthropological Sciences*, *12*(8), 190. https://doi.org/10.1007/s12520-020-01140-z
19. Garcia Guinea, J., Correcher, V., & Valle-Fuentes, F. J. (1999). Thermoluminescence of Kaolinite. *Radiation Protection Dosimetry*, *84*(1), 507–510. https://doi.org/10.1093/oxfordjournals.rpd.a032787
20. Garzón, E., Pérez-Villarejo, L., Eliche-Quesada, D., Martínez-Martínez, S., & Sánchez-Soto, P. J. (2022). Vitrification rate and estimation of the optimum firing conditions of ceramic materials from raw clays: A review. *Ceramics International*, *48*(11), 15889–15898. https://doi.org/10.1016/j.ceramint.2022.02.129
21. Ghale, D. B., Bohara, N. B., . Duwal, N., & . Bhattarai, J. (2019). Investigation on the mineralogical phase of ancient brick samples of Kathmandu Valley (Nepal) using XRD and FTIR analysis. *Rasayan Journal of Chemistry*, *12*(02), 402–408. https://doi.org/10.31788/RJC.2019.1224034
22. Goldstein, J. I., Newbury, D. E., Echlin, P., Joy, D. C., Lyman, C. E., Lifshin, E., Sawyer, L., & Michael, J. R. (2003). *Scanning Electron Microscopy and X-ray Microanalysis: Third Edition*. Springer US. https://doi.org/10.1007/978-1-4615-0215-9
23. Govindasamy, A., Viruthagiri, G., & Ramesh, K. (2019a). FI-IR Spectroscopic and Porosity Studies to Estimate the Firing Temperature of the Clay Brick. 14(12).
24. Govindasamy, A., Viruthagiri, G., & Ramesh, K. (2019b). FI-IR Spectroscopic and Porosity Studies to Estimate the Firing Temperature of the Clay Brick. 14(12), 2904–2909.
25. Grim, R. E. (1968). *Clay mineralogy* (2nd Ed). McGraw Hill.
26. Hajjaji, M., Kacim, S., Alami, A., El Bouadili, A., & El Mountassir, M. (2001). Chemical and mineralogical characterization of a clay taken from the Moroccan Meseta and a study of the interaction between its fine fraction and methylene blue. *Applied Clay Science*, *20*(1), 1–12. https://doi.org/10.1016/S0169-1317(00)00041-7
27. Hayashi, H., Otsuka, R., & Imai, N. (1969). Infrared study of sepiolite and paly-gorskite on heating. *American Mineralogist*, *54*(11–12), 1613–1624.
28. Hindy, K., Baghdady, A., M. Howari, F., & Abdelmaksoud, A. (2018). A Qualitative Study of Airborne Minerals and Associated Organic Compounds in Southeast of Cairo, Egypt. *International Journal of Environmental Research and Public Health*, *15*(4), 568. https://doi.org/10.3390/ijerph15040568
29. Hlavay, J., Jonas, K., Elek, S., & Inczedy, J. (1978). Characterization of the Particle Size and the Crystallinity of Certain Minerals by IR Spectrophotometry and other Instrumental Methods—II. Investigations on Quartz and Feldspar. *Clays and Clay Minerals*, *26*(2), 139–143. https://doi.org/10.1346/CCMN.1978.0260209
30. Huntley, D. J., & Lamothe, M. (2001). Ubiquity of anomalous fading in K-feldspars and the measurement and correction for it in optical dating. *Canadian Journal of Earth Sciences*, *38*(7), 1093–1106. https://doi.org/10.1139/e01-013

 doi:10.20944/preprints202406.0997.v1

31. Iordanidis, A., Garcia-Guinea, J., & Karamitrou-Mentessidi, G. (2009). Analytical study of ancient pottery from the archaeological site of Aiani, northern Greece. *Materials Characterization*, *60*(4), 292–302. https://doi.org/10.1016/j.matchar.2008.08.001
32. İssi, A., Kara, A., & Alp, A. O. (2011). An investigation of Hellenistic period pottery production technology from Harabebezikan/Turkey. *Ceramics International*, *37*(7), 2575–2582. https://doi.org/10.1016/j.ceramint.2011.04.001
33. Job Ajala, A., Badarulzaman, N. A., & Aramjat, A. B. (2017). Impact of Sintering Temperatures on Microstructure, Porosity and Mechanical Strength of Refractory Brick. *Materials Science Forum*, *888*, 66–70. https://doi.org/10.4028/www.scientific.net/MSF.888.66
34. Job Ajala, A., Nur Azam, B., & Abu Bakar, A. (2016). Influence of Sintering Temperatures on Physico-Mechanical Properties and Microstructure of Refractory Fireclay Bricks. *International Journal of Engineering and Technology*, *8*(6), 2588–2593. https://doi.org/10.21817/ijet/2016/v8i6/160806214
35. Johari, I., Said, S., Hisham, B., Bakar, A., & Ahmad, Z. A. (2010). Effect of the change of firing temperature on microstructure and physical properties of clay bricks from Beruas (Malaysia). *Science of Sintering*, *42*(2), 245–254. https://doi.org/10.2298/SOS1002245J
36. Jozanikohan, G., & Abarghooei, M. N. (2022). The Fourier transform infrared spectroscopy (FTIR) analysis for the clay mineralogy studies in a clastic reservoir. *Journal of Petroleum Exploration and Production Technology*, *12*(8), 2093–2106. https://doi.org/10.1007/s13202-021-01449-y
37. Karaman, S., Erşahin, S., & Günal, H. (2006). Firing temperature and firing time influence on mechanical and physical properties of clay bricks. *Journal of Scientific & Industrial Research*. https://www.semanticscholar.org/paper/Firing-temperature-and-firing-time-influence-on-and-Karaman-Er%C5%9Fahin/f0cf8fe0caf2127e9b95492b85981a3292925d16
38. Keller, W. D., & Pickett, E. E. (1949). Absorption of infrared radiation by powdered silica minerals. *American Mineralogist*, *34*(11–12), 855–868.
39. Kiruba, S., & Ganesan, S. (2015). FT-IR and Micro-Raman spectroscopic studies of archaeological potteries recently excavated in Poompuhar, Tamilnadu, India. *Spectrochimica Acta Part A: Molecular and Biomolecular Spectroscopy*, *145*, 594–597. https://doi.org/10.1016/j.saa.2015.03.055
40. Lecomte, G., Pateyron, B., & Blanchart, P. (2004). Experimental study and simulation of a vertical section mullite-ternary eutectic (985°C) in the SiO2–Al2O3–K2O system. *Materials Research Bulletin*, *39*(10), 1469–1478. https://doi.org/10.1016/j.materresbull.2004.04.024
41. Legodi, M. A., & De Waal, D. (2007). Raman spectroscopic study of ancient South African domestic clay pottery. *Spectrochimica Acta Part A: Molecular and Biomolecular Spectroscopy*, *66*(1), 135–142. https://doi.org/10.1016/j.saa.2006.02.059
42. Leriche, A., Cambier, F., & Hampshire, S. (2017). Sintering of Ceramics. In *Reference Module in Materials Science and Materials Engineering* (p. B9780128035818102887). Elsevier. https://doi.org/10.1016/B978-0-12-803581-8.10288-7
43. Libretexts. (2014, November 30). *Infrared Spectroscopy Absorption Table*. Chemistry LibreTexts. https://chem.libretexts.org/Ancillary_Materials/Reference/Reference_Tables/Spectroscopic_Reference_Tables/Infrared_Spectroscopy_Absorption_Table
44. Lindholm, R. C. (1987). *A Practical Approach to Sedimentology*. Springer Netherlands. https://doi.org/10.1007/978-94-011-7683-5
45. Lyon, R. J. P. (1967). Infrared absorption spectroscopy, physical methods in determinative mineralogy. (Zussman J, pp. 371–403). Academic Press.
46. Maniatis, Y., Katsanos, A., & Caskey, M. E. (1982). Technological Examination of Low-Fired Terracotta Statues from Ayia Irini, Kea. *Archaeometry*, *24*(2), 191–198. https://doi.org/10.1111/j.1475-4754.1982.tb01001.x
47. Maniatis, Y., Simopoulos, A., Kostikas, A., & Perdikatsis, V. (1983). Effect of reducing atmosphere on minerals and iron oxides developed in fired clays: The role of Ca. *Journal of the American Ceramic Society*, *66*(11), 773–781.
48. Maniatis, Y., & Tite, M. S. (1978). *Ceramic Technology in the Aegan world during the Bronze Age* (C. Doumas, Ed.; Vol. 1). Thera and the Aegan world.
49. Maniatis, Y., & Tite, M. S. (1981). Technological examination of Neolithic-Bronze Age pottery from central and southeast Europe and from the Near East. *Journal of Archaeological Science*, *8*(1), 59–76. https://doi.org/10.1016/0305-4403(81)90012-1
50. Maritan, L., Nodari, L., Mazzoli, C., Milano, A., & Russo, U. (2006). Influence of firing conditions on ceramic products: Experimental study on clay rich in organic matter. *Applied Clay Science*, *31*(1–2), 1–15. https://doi.org/10.1016/j.clay.2005.08.007
51. Mendelovici, E. (1997). Comparative study of the effects of thermal and mechanical treatments on the structures of clay minerals. *Journal of Thermal Analysis*, *49*(3), 1385–1397. https://doi.org/10.1007/BF01983697
52. Miller, J. G. (1961). Infrared investigations of clay related minerals. 63, 80.

53. Mostaghelchi, M., Zahiri, R., Miremad, S. H., & Ebadi, A. G. (2013). Use of Mica Mineral Powder in Bricks Industry to Improve the Performances. *Asian Journal of Chemistry*, *25*(16), 9144–9148. https://doi.org/10.14233/ajchem.2013.15053C
54. Murray, A. S., & Roberts, R. G. (1998). Measurement of the equivalent dose in quartz using a regenerative-dose single-aliquot protocol. *Radiation Measurements*, *29*(5), 503–515. https://doi.org/10.1016/S1350-4487(98)00044-4
55. Osborn, E. F., & Muan, A. (1960). *Phase equilibrium diagrams of oxide systems*. American Ceramic Society with the Edward Orton Jr. Ceramic Foundation.
56. Panzeri, L., Galli, A., Maspero, F., Saleh, M., & Martini, M. (2022). The activities of the LAMBDA (Laboratory of Milano Bicocca university for Dating and Archaeometry): What's new? *Journal of Physics: Conference Series*, *2204*(1), 012047. https://doi.org/10.1088/1742-6596/2204/1/012047
57. Papachristodoulou, C., Oikonomou, A., Ioannides, K., & Gravani, K. (2006). A study of ancient pottery by means of X-ray fluorescence spectroscopy, multivariate statistics and mineralogical analysis. *Analytica Chimica Acta*, *573–574*, 347–353. https://doi.org/10.1016/j.aca.2006.02.012
58. Polymeris, G. S., Kitis, G., Afouxenidis, D., Sfampa, I. K., Tsirliganis, N. C., Rousaki, A., Kouloumpi, E., & Paraskevopoulos, K. M. (2013). On the feasibility of dating portable paintings: Preliminary luminescence measurements on ground materials. *Mediterranean Archaeology and Archaeometry*, *13*(3), 93–103.
59. Prescott, J. R., & Hutton, J. T. (1994). Cosmic ray contributions to dose rates for luminescence and ESR dating: Large depths and long-term time variations. *Radiation Measurements*, *23*(2–3), 497–500. https://doi.org/10.1016/1350-4487(94)90086-8
60. Raja Annamalai, G., Ravisankar, R., Rajalakshmi, A., Chandrasekaran, A., & Rajan, K. (2014). Spectroscopic characterization of recently excavated archaeological potsherds from Tamilnadu, India with multi-analytical approach. *Spectrochimica Acta Part A: Molecular and Biomolecular Spectroscopy*, *133*, 112–118. https://doi.org/10.1016/j.saa.2014.04.188
61. Ramasamy, K., & Kamalakkannan, V. (1987). Infrared study of some South Indian Clays. *Indian Journal of Pure and Applied Physics*, *25*, 284–286.
62. Ramasamy, V., Murugesan, S., & Mullainathan, S. (2004). Characterisation of minerals and relative distribution of quartz in Cauvery river sediments from Tamilnadu, India – A FTIR Study. *Bulletin of Pure and Applied Sciences*, *23F*(1 & 2), 1–7.
63. Ramasamy, V., Rajkumar, P., & Ponnusamy, V. (2009). Depth wise analysis of recently excavated Vellar river sediments through FTIR and XRD studies. 83(9), 1295–1308.
64. Rasmussen, K. L., De La Fuente, G. A., Bond, A. D., Mathiesen, K. K., & Vera, S. D. (2012). Pottery firing temperatures: A new method for determining the firing temperature of ceramics and burnt clay. *Journal of Archaeological Science*, *39*(6), 1705–1716. https://doi.org/10.1016/j.jas.2012.01.008
65. Ravisankar, R., Kiruba, S., Naseerutheen, A., Chandrasekaran, A., Annamalai, G. R., Seran, M., & Balaji, P. D. (2011). Estimation of the firing temeparaure of arachaelocigical pottery excavated from Thiruverkadu, Tamilnadu, India by FT-IR spectroscopy.
66. Ravisankar, R., Kiruba, S., Shamira, C., Naseerutheen, A., Balaji, P. D., & Seran, M. (2011). Spectroscopic techniques applied to the characterization of recently excavated ancient potteries from Thiruverkadu Tamilnadu, India. *Microchemical Journal*, *99*(2), 370–375. https://doi.org/10.1016/j.microc.2011.06.012
67. Ravisankar, R., Naseerutheen, A., Rajalakshmi, A., Raja Annamalai, G., & Chandrasekaran, A. (2014). Application of thermogravimetry–differential thermal analysis (TG–DTA) technique to study the ancient potteries from Vellore dist, Tamilnadu, India. *Spectrochimica Acta Part A: Molecular and Biomolecular Spectroscopy*, *129*, 201–208. https://doi.org/10.1016/j.saa.2014.02.095
68. Ravisankar, R., Raja Annamalai, G., Naseerutheen, A., Chandrasekaran, A., Prasad, M. V. R., Satpathy, K. K., & Maheswaran, C. (2013). Analytical characterization of recently excavated megalithic sarcophagi potsherds in Veeranam village, Tiruvannamalai dist., Tamilnadu, India. *Spectrochimica Acta Part A: Molecular and Biomolecular Spectroscopy*, *115*, 845–853. https://doi.org/10.1016/j.saa.2013.06.123
69. Ravisankar, R., Raja Annamalai, G., Rajan, K., Naseerutheen, A., & Senthil Kumar, G. (2012). Mineral Analysis In Archaeological Pottery From Porunthal, Dindigal Dist, Tamilnadu, India By FT-IR Spectroscopic Technique. *International Journal of Science Innovations and Discoveries*, *2*(1), 53–60.
70. Russ, W., Mörtel, H., & Meyer-Pittroff, R. (2005). Application of spent grains to increase porosity in bricks. *Construction and Building Materials*, *19*(2), 117–126. https://doi.org/10.1016/j.conbuildmat.2004.05.014
71. Russell, J. D. (1987). Infrared methods. In *A Handbook of Determinative Methods in Clay Mineralogy* (M.J.Wilson, p. 133). Blackie and Sons Ltd.,.
72. Rutherford, J. S., Almond, M. J., & Nunn, P. D. (2012). Analysis of pottery samples from Bourewa, the earliest known Lapita site in Fiji. *Spectrochimica Acta Part A: Molecular and Biomolecular Spectroscopy*, *85*(1), 155–159. https://doi.org/10.1016/j.saa.2011.09.050
73. Sánchez-Soto, P. J., Garzón, E., Pérez-Villarejo, L., & Eliche-Quesada, D. (2023). Sintering behaviour of a clay containing pyrophyllite, sericite and kaolinite as ceramic raw materials: Looking for the optimum

firing conditions. *Boletín de La Sociedad Española de Cerámica y Vidrio*, *62*(1), 26–39. https://doi.org/10.1016/j.bsecv.2021.09.001

74. Seetha, D., & Velraj, G. (2016). Characterization and chemometric analysis of ancient pot shards trenched from Arpakkam, Tamil Nadu, India. *Journal of Applied Research and Technology*, *14*(5), 345–353. https://doi.org/10.1016/j.jart.2016.08.002
75. Serna, C., VanScoyoc, G. E., & Ahlrichs, J. L. (1977). Hydroxyl groups and water in palygorskite. *American Mineralogist*, *62*(7–8), 784–792.
76. Sheikh, M. R. (2017a). Physics for Cultural Heritage: TL Dating of the Kamakhya Temple, Assam, India. *3*(4), 174–176.
77. Sheikh, M. R. (2017b). Physics for Cultural Heritage: TL Dating of the Kamakhya Temple, Assam, India. *International Journal of Current Trends in Engineering & Technology*, *3*(4), 174–176.
78. Sheikh, M. R., & Barua, A. G. (2013). X-ray diffraction and Fourier transform infrared spectra of the bricks of the Kamakhya temple. 15(11), 745–748.
79. Shillito, L. M., Almond, M. J., Wicks, K., Marshall, L.-J. R., & Matthews, W. (2009). The use of FT-IR as a screening technique for organic residue analysis of archaeological samples. *Spectrochimica Acta Part A: Molecular and Biomolecular Spectroscopy*, *72*(1), 120–125. https://doi.org/10.1016/j.saa.2008.08.016
80. Shoval, S. (1994). The firing temperature of a persian-period pottery kiln at Tel Michal, Israel, estimated from the composition of its pottery. *Journal of Thermal Analysis*, *42*(1), 175–185. https://doi.org/10.1007/BF02546999
81. Song, Z., Chouparova, E., Jones, K., Feng, H., & Marinkovic, N. (2001). *FTIR Investigation of Sediments from NY/NJ Harbor, San Diego Bay, and the Venetian Lagoon*. https://www.semanticscholar.org/paper/FTIR-Investigation-of-Sediments-from-NY-NJ-Harbor%2C-Song-Chouparova/1250a3c0eb8080def771f168978dd5fcc2091905
82. Theodosoglou, E., Koroneos, A., Soldatos, T., Zorba, T., & Paraskevopoulos, K. M. (2010). Comparative Fourier transform infrared and X-ray powder diffraction analysis of naturally occurred K-feldspars. *Bulletin of the Geological Society of Greece*, *43*(5), Article 5. https://doi.org/10.12681/bgsg.11681
83. Tite, M. S. (1992). The Impact of Electron Microscopy on Ceramic Studies. *Proceedings of the British Academy*, *77*, 111–131.
84. Tite, M. S., & Maniatis, Y. (1975). Examination of ancient pottery using the scanning electron microscope. *Nature*, *257*(5522), Article 5522. https://doi.org/10.1038/257122a0
85. Tucker, M. (1988). *Techniques in sedimentology*. https://www.semanticscholar.org/paper/Techniques-in-sedimentology-Tucker/8f7d146ef7f60092851570958bf1d81525820305
86. Velraj, G., Janaki, K., Musthafa, A. M., & Palanivel, R. (2009). Estimation of firing temperature of some archaeological pottery shreds excavated recently in Tamilnadu, India. *Spectrochimica Acta Part A: Molecular and Biomolecular Spectroscopy*, *72*(4), 730–733. https://doi.org/10.1016/j.saa.2008.11.015
87. Velraj, G., Sathya, P., Champion, P. M., & Ziegler, L. D. (2010). *Mineralogical Appraisal Of Ancient Brick Samples Using FT-IR Spectroscopy*. 307–308. https://doi.org/10.1063/1.3482527
88. Velraj, G., Seetha, D., & Hemamalini, R. (2014). FT-IR, XRD, Porosity and TG-DTA Analysis of Archaeological Potteries Excavated from Kottapuram, Kerala, South India. 66, 20815–20819.
89. Weaver, M. E. (1997). *Conserving Buildings: Guide to Techniques and Materials, Revised Edition*. John Wiley & Sons, Inc. https://www.biblio.com/book/conserving-buildings-guide-techniques-materials-revised/d/1573100919
90. Wintle, A. G. (1973). Anomalous Fading of Thermo-luminescence in Mineral Samples. *Nature*, *245*(5421), Article 5421. https://doi.org/10.1038/245143a0
91. Zimmerman, D. W. (1971). Thermoluminescence dating using fine grains from pottery. *Archaeometry*, *13*(1), 29–52. https://doi.org/10.1111/j.1475-4754.1971.tb00028.x